SUPPLEMENTARY MATERIAL

1 An iterative approach for wet-bulb temperature calculation

The wet-bulb temperature is an important variable in thermodynamics. However, there exists no simple direct mathematical formula for calculating the wet-bulb temperature as a function of the dry-bulb temperature (θ_{db} [°C] or T_{db} [K]) and the relative humidity (φ_a [%]) (Knox et al., 2017). (Stull, 2011) developed an empirical equation based on gene-expression programming to directly calculate the wet-bulb temperature (θ_{wb} [°C] or T_{wb} [K]) from the dry-bulb temperature ([-20, 50] °C) and relative humidity ([0, 100] %). However, in this range, the mean absolute error for the wet-bulb temperature, in comparison to the values reported in the psychrometric chart, was reported as 0.28 °C, with errors in some predictions as high as ± 0.65 °C.

This error is relatively large when considering temperature differences, such as the wet-bulb depression, i.e., $\Delta T_{ev} = T_{db} - T_{wb}$, which is typically a few degrees Celcius. This depression is the maximum drop in temperature that can be achieved due to evaporative cooling. The wet-bulb depression can be quite small, especially for regions with a high dry-bulb temperature and low relative humidity, which is the typical climate in hot and dry deserts. To minimize this error in predicting wet-bulb temperature, we used an iterative approach to calculate the wet-bulb temperature using the dry-bulb temperature and the relative humidity of the air. First, we define moist air properties below and derive the wet-bulb temperature in the next section.

Moist air properties

Moist air (subscript a) is considered to be a mixture of two ideal gasses, namely dry air (subscript d) and water vapor (subscript v). The ideal gas law can be defined for each of these mixture components:

$$\begin{aligned} p_d &= \rho_d R_d T = \frac{m_d}{V_a} R_d T = x_d \rho_a R_d T \\ p_v &= \rho_v R_v T = \frac{m_v}{V_a} R_v T = x_v \rho_a R_v T \end{aligned} \tag{1}$$

Here p_d and p_v are partial pressures [Pa], i.e., the dry air and water vapor pressure, R_d and R_v are specific gas constants [J $kg^{-1}K^{-1}$], ρ_d and ρ_v are densities [kg m^{-3}], m_d and m_v are masses [kg], and x_d and x_v are mass fractions of dry air and water vapor [kg kg^{-1}], respectively. V_a is the volume of the mixture (moist air) [m^3], ρ_a is the mixture density [kg m^{-3}], and T is the temperature of the mixture [K], since thermal equilibrium between all mixture components is assumed, by which $T_d = T_v = T_a = T$. The mass fractions define as and related by:

$$\begin{aligned} x_d &= \frac{m_d}{m_a} = \frac{\rho_d}{\rho_a} \\ x_v &= \frac{m_v}{m_a} = \frac{\rho_v}{\rho_a} \\ x_d + x_v &= 1 \end{aligned} \tag{2}$$

The density of the mixture (ρ_a [kg_a m_a^{-3}]) is thereby related to the density of its components dry air (ρ_d [kg_d m_a^{-3}]) and water vapor (ρ_v [kg_v m_a^{-3}]) by:

$$\begin{aligned} \rho_d &= \frac{m_d}{V_a} = x_a \rho_a \\ \rho_v &= \frac{m_v}{V_a} = x_v \rho_a \end{aligned} \tag{3}$$

Here, ρ_v is also called absolute humidity. The following relations connect the three gasses:

$$\begin{aligned} \rho_a &= \rho_d + \rho_v \\ x_d + x_v &= 1 \end{aligned} \tag{4}$$

The specific gas constants R_d (287.044 J $kg^{-1}K^{-1}$) and R_v (461.524 J $kg^{-1}K^{-1}$) are determined from the universal gas constant R (8.31451 J $mol^{-1}K^{-1}$), and the molecular masses M_d and M_v of dry air (28.966 g mol^{-1}) and water vapor (18.01534 g mol^{-1}) by:

$$R_d = \frac{R}{M_d}$$
$$R_v = \frac{R}{M_v} \tag{5}$$

Dalton's law states that the total pressure of a mixture (p_a), in this case, moist air, is the sum of the partial pressures of the components:

$$p_a = p_d + p_v \tag{6}$$

If we combine these equations, the total pressure can also be written as:

$$p_a = p_d + p_v = \rho_a RT\left(\frac{x_d}{M_d} + \frac{x_v}{M_v}\right) = \rho_a RT\frac{1}{M_a} \tag{7}$$

Here M_a is the molecular mass of the mixture. The air density is around 1.2 kg $m^{-3,}$ and the air pressure equals the atmospheric pressure (P_{atm}), which is taken equal to 101 325 Pa. At low wind speeds (< ± 110 m s^{-1}), i.e., at Mach numbers below 0.3, the air is usually assumed to be incompressible. This means that pressure variations are sufficiently small to have no significant effect on the density. However, the influence of (small) variations in temperature and vapor concentration on the (moist) air density is still accounted for using the ideal gas law.

The vapor fraction or specific humidity [kg_v kg_a^{-1}] is often rewritten as a direct function of the vapor pressure:

$$x_v = \frac{p_v}{\rho_a R_v T} = \frac{p_v}{\frac{p_a}{R_a T}R_v T} = \frac{p_v}{\frac{p_a}{R_a}R_v} = \frac{R_a}{R_v}\frac{p_v}{p_a} = \frac{\frac{R}{M_a}}{\frac{R}{M_v}}\frac{p_v}{p_a} = \frac{M_v}{M_a}\frac{p_v}{p_a} \approx \frac{M_v}{M_d}\frac{p_v}{p_a} = 0.622\frac{p_v}{p_a} = \varepsilon\frac{p_v}{P_{atm}} \tag{8}$$

Here ε is the ratio of molecular weights of water vapor and dry air (0.622 kg_v kg_d^{-1}). Note that often the specific humidity (x_v' [kg_v kg_d^{-1}]) is defined in units of dry air (Appropedia, 2021). This is a reasonable approximation since:

$$x_v' = \frac{m_v}{m_d} = \frac{\frac{p_v V_a}{R_v T}}{\frac{p_d V_a}{R_d T}} = \frac{R_d p_v}{R_v p_d} = 0.622\frac{p_v}{p_d} \approx 0.622\frac{p_v}{p_a} = x_v = \varepsilon\frac{p_v}{P_{atm}} \tag{9}$$

$$\text{with } m_v = \frac{p_v V_a}{R_v T}; m_d = \frac{p_d V_a}{R_d T} \tag{10}$$

Other derived parameters are relative humidity φ [%] and saturated vapor pressure $p_{v,sat}$ [Pa]. The saturated vapor can be calculated using many different empirical equations with very similar results (Allen et al., 1998; Defraeye and Radu, 2017):

$$\varphi = \frac{p_v(T)}{p_{v,sat}(T)} \tag{11}$$

$$p_{v,sat}(T) = 610.8e^{\left(\frac{17.27\theta}{\theta+237.3}\right)} \tag{12}$$

$$p_{v,sat}(T) = e^{65.8094 - \frac{7066.27}{T} - 5.976\ln(T)} \tag{13}$$

Wet-bulb temperature

The wet-bulb temperature is the temperature that a parcel of air would have if it is adiabatically cooled to saturation by evaporation of water, assuming all latent heat is supplied by the air parcel and at constant pressure. If we apply the first law of the thermodynamics to an air parcel comprising 1 kg dry air and x_v' kg of water vapor (so specific humidity is x_v' [$kg_v\ kg_d^{-1}$]) and experience the above process, we arrive at the equation:

$$\int_{T_{db}}^{T_{wb}} c_{p,a}(1+x_v')\,dT = \int_{x_{v,db}'}^{x_{v,sat,wb}'} L_v^{\text{ref}}\,dx_v' \tag{14}$$

where L_v^{ref} is the latent heat of vaporization [J kg_l^{-1}], $x_{v,db}'$ is the specific humidity of the air parcel corresponding to the dry bulb temperature [$kg_v\ kg_d^{-1}$], $x_{v,sat,wb}'$ is the saturated specific humidity at the wet-bulb temperature [$kg_v\ kg_d^{-1}$], $c_{p,a}$ is the isobaric specific heat capacity of the moist air [J $kg^{-1}\ K^{-1}$]. The specific heat capacity of the moist air can be expressed as the sum of the contributions of the specific heat capacity of dry air ($c_{p,d}$) and water vapor ($c_{p,v}$) as:

$$c_{p,a}(1+x_v') = c_{p,d}(1) + c_{p,v}(x_v') \tag{15}$$

If we integrate Eq.(14) and replace the term using Eq.(15), and represent the difference between dry-bulb and wet-bulb temperature as wet-bulb depression (ΔT_{ev}), we get:

$$\Delta T_{ev} = T_{db} - T_{wb} = \frac{(x_{v,sat,wb}' - x_{v,db}')L_v^{\text{ref}}}{c_{p,d}(1) + c_{p,v}(x_v')} \tag{16}$$

Since the specific humidity x_v' is normally <<1 (lying between 0 and 0.03 $kg_v\ kg_d^{-1}$ in the psychrometric chart), we can assume that the term $(c_{p,d}+c_{p,v}\cdot x_v')\approx c_{p,d}$, so the wet-bulb depression takes the form:

$$\Delta T_{ev} = \frac{(x_{v,sat,wb}' - x_{v,db}')L_v^{\text{ref}}}{c_{p,d}} \tag{17}$$

Additionally, if we replace $x_{v,sat,wb}'$ and $x_{v,db}'$ by the approximation in Eq.(9), we get:

$$\Delta T_{ev} = \frac{0.622(p_{v,sat} - p_v)}{P_{atm}}\frac{L_v^{\text{ref}}}{c_{p,d}} = \frac{(p_{v,sat} - p_v)}{P_{atm}}\frac{\varepsilon L_v^{\text{ref}}}{c_{p,d}} = \frac{(p_{v,sat} - p_v)}{P_{atm}}\frac{1}{\gamma} \tag{18}$$

Here γ is is the psychrometric constant ($(c_{p,d}/(\varepsilon.L_v^{ref})) \approx 0.65 \times 10^{-3}\ K^{-1}$) (Simões-Moreira, 1999). This parameter can be assumed to be constant as long the assumption x_v' <<1 is valid.

If we now rearrange Eq.(18) and consider the psychrometric constant, we obtain Eq.(19):

$$p_v\langle T_{db}\rangle - p_{v,sat}\langle T_{wb}\langle T_{db}, \varphi_a\rangle\rangle + \gamma\, P_{\text{atm}}(T_{db} - T_{wb}) = 0 \tag{19}$$

We solve this equation iteratively to obtain the wet-bulb temperature so that the error in the predicted wet-bulb temperature satisfying this equation is < 0.001 K. The procedure is depicted graphically in Figure 1. We used Eq.(12) to compute the vapor pressure (Pa) as a function of temperature (in °C). With this approach, the relative deviation for wet-bulb temperature was within ±0.4% in comparison to the values measured using a psychrometer when θ_{wb} < 30 °C (Simões-Moreira, 1999).

The initial guess for the wet-bulb temperature ($\theta_{wb,guess\_0}$, °C) was derived as an approximation from the dew point temperature (θ_{dew},°C) and the dry-bulb temperature (θ_{db}, °C) (Knox et al., 2017). This was merely used as an approximation to obtain the initial guess for the wet-bulb temperature to reduce computational time, as it is quite widely acknowledged that the wet-bulb temperature lies somewhere between the dew-point temperature and the dry-bulb temperature (Knox et al., 2017).

$$\theta_{\text{wb,guess\_0}} = \frac{\gamma\theta_{db} + \Delta S \cdot \theta_{\text{dew}}}{\gamma + \Delta S} \tag{20}$$

ΔS is the slope of saturation vapor pressure at the dew point temperature:

$$\Delta S = \frac{4098 \times p_{v,a}}{(\theta_{\text{dew}} + 237.3)^2} \tag{21}$$

The dew point (θ_{dew}, °C) was computed from the ambient vapor pressure (p_v [Pa]) using Eq.(22).

$$\theta_{\text{dew}} = \frac{116.9 + 237.3\ln(p_v)}{16.78 - \ln(p_v)} \tag{22}$$

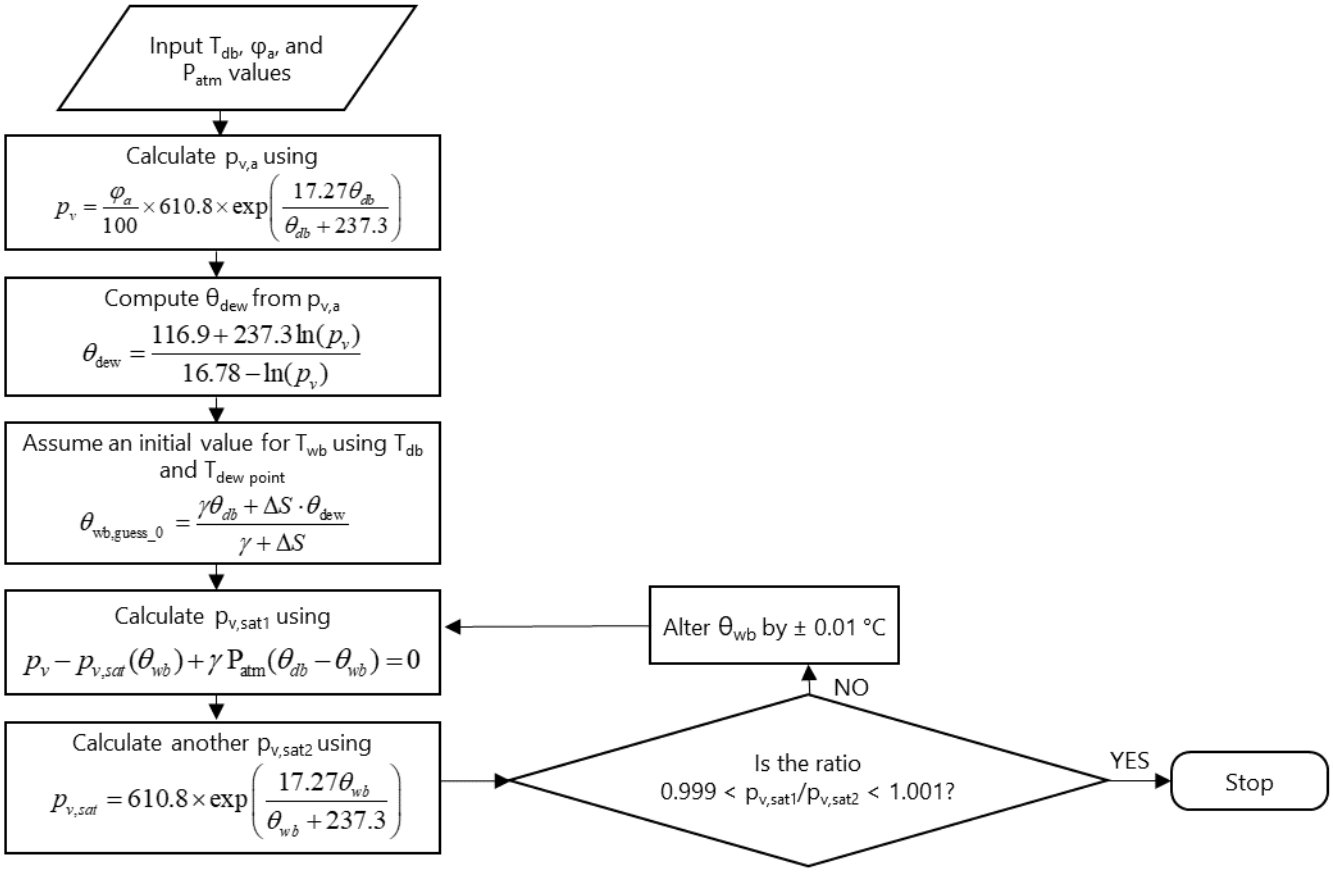

Figure 1. Flow diagram for the iterative solution of wet-bulb temperature from the dry-bulb temperature (T_{db}, °C) and relative humidity (φ_a). P_{atm} = atmospheric pressure (Pa); p_v = vapor pressure of ambient air (Pa); θ_{db} = dry-bulb temperature (in °C); θ_{dew} = dew point temperature (in °C); $\theta_{wb,guess\_0}$ = initial guess for wet-bulb temperature (in °C); $p_{v,sat}$ = saturated vapor pressure (Pa).

2 Kinetic quality models for postharvest life of fruit

The maximal gain in postharvest life is calculated by comparing the postharvest life when fruit are stored at the dry-bulb temperature (T_{db}) and at the corresponding wet-bulb temperature (T_{wb}), so in an idealized evaporative cooler. We do this calculation for any given set of T_{db} and φ_a.

The respiration-driven quality evolution of fruit is modeled with a first-order kinetic rate law model (n = 1), which calculated the overall fruit quality index (I, %) (Tijskens and Polderdijk, 1996).

$$-\frac{dI}{dt} = k_{fr}(T) \cdot I(\text{t})^{\text{n}} \tag{23}$$

Here, I represents the respiration-driven fruit quality index [%] and k_{fr} is the temperature-dependent rate constant [s^{-1}]. In this equation, this temperature corresponds to T_{db} for the postharvest life calculation in the absence of evaporative cooling and T_{wb} for a case where fruits are subject to evaporative cooling and achieve the maximal temperature reduction that is possible. The initial fruit quality at the time of harvest (I_0) is assumed to be 100%. In

this study, the threshold for loss of fruit quality (I_{thr}) was set to 10%. We assumed that below this value, fruits are no longer marketable.

The temperature dependence of the rate constant k_{fr} [s^{-1}] was accounted for using the Arrhenius equation.

$$k_{fr}(T) = k_{0,fr} \exp\left(\frac{-E_{a,fr}}{R.T}\right) \tag{24}$$

where $k_{0,fr}$ is the pre-exponential reference rate constant [s^{-1}], $E_{a,fr}$ is the activation energy [J mol^{-1}], and R corresponds to the universal gas constant (8.314 J mol^{-1} K^{-1}). The values of $k_{0,f,}$ and $E_{a,fr}$ were determined based on the optimal storage conditions and the coefficient Q_{10} for every fruit (Defraeye et al., 2019; Shoji et al., 2022). The $Q_{10,fr}$ value for a fruit corresponds to the ratio between the rate constants of degradation reaction in the food at different temperatures. Q_{10} typically lies between 2 and 3 for most fresh produce (Robertson, 2016).

$$Q_{10,fr} = \frac{k_{fr}(T+10)}{k_{fr}(T)} \tag{25}$$

The optimal storage conditions, values of $Q_{10,fr}$, and the parameters of the kinetic quality models are detailed in Table 1. The postharvest life (PL_{fr} [days]) at any given temperature T, starting from fruit at a quality index I_{ini}, is determined as from the kinetic quality model. Here we age the fruit in the model virtually at a constant temperature, starting from I_{ini} until it reaches the threshold quality index I_{thr}.

$$PL_{fr}(T) = \frac{\ln(I_{ini} / I_{thr})}{k_{fr}(T)} \tag{26}$$

Note that the initial quality index I_{ini} for this calculation can be the initial fruit quality at the time of harvest (I_0) but also any intermediate quality in the supply chain from which the remaining postharvest life is calculated. If the postharvest life is calculated at shelf-life conditions, it is the remaining shelf life.

The maximal gain in postharvest life due to evaporative cooling is computed as the difference in postharvest life when fruit are stored at (constant) wet-bulb temperature versus at (constant) dry-bulb temperature. Therefore, it corresponds to the additional days gained by storing the fruit in the evaporative cooler at wet-bulb temperature conditions, as opposed to storing fruit in shaded ambient dry-bulb temperature conditions. This gain in postharvest life is based on the maximal possible reduction in temperature due to evaporative cooling.

$$\Delta PL_{fr} = PL_{fr}(T_{wb}\langle T_{db}, \varphi_a \rangle) - PL_{fr}(T_{db}) \tag{27}$$

This calculation does not account for the increase in postharvest life due to the reduced moisture loss as a consequence of the increased relative humidity in the evaporative cooler. ΔPL_{fr} is the maximal gain in postharvest life that is achieved under ideal conditions. However, in reality, ΔPL_{fr} might be lower as the wet-bulb temperature is not exactly reached by evaporative cooling.

In some regions in the world, T_{db} or T_{wb} are lower than the optimal temperature to store produce. For example, in the case of banana fruit, the optimal storage temperature is about 14°C (Camelo, 2004). In case T_{db} or T_{wb} are lower than the optimal storage temperature of the fruit, we replaced these temperatures for the calculations with the optimal temperature to store that produce. We thus assume that the optimal storage conditions can be implemented on-site. Thus, for bananas, a dry-bulb or wet-bulb temperature lower than 14 °C is replaced by 14 °C. If both temperatures are lower, they are set at the same value. As a result, no gain in shelf life will be achieved when placing the fruit in the evaporative cooler. This thresholding is done to avoid predicting a postharvest life that is longer than that under the optimal conditions. For some fresh produce, temperatures much lower than the optimal temperature can be detrimental to fruit quality, for example, by causing chilling injury to the fruit.

Table 1. Optimal storage conditions and parameters for the kinetic quality models employed for calculating the gain in postharvest life due to evaporative cooling for apple, banana, mango, and tomato.

Fruit	**Optimal storage temperature [°C]**	**Postharvest life at optimal temperature [d]**	**Q_{10} value [-]**	**Activation energy [kJ mol^{-1}]**	**Pre-exponential rate constant [s^{-1}]**	**Reference**
Apple	1.5	115.0	3	70.66	6.386 x 10^{6}	(Cantwell, 2001; Eissa et al., 2017)
Banana	14.0	17.5	2	44.58	1.965 x 10^{2}	(Cantwell, 2001; Kole and Prasad, 1994)
Mango	13.0	17.5	3	70.66	1.210 x 10^{7}	(Cantwell, 2001; Defraeye et al., 2019)
Tomato	9.0	9.0	2	44.58	5.320 x 10^{2}	(Cantwell, 2001)

3 GIS maps of India and the rest of the world

3.1 GIS and climate data

We describe how we obtained GIS maps of the maximal gain in postharvest life that can be achieved by evaporative cooling. We illustrate the workflow for India and later compose the map for the entire world. First, we obtained the climate data from the ERA5 database. ERA5 is the fifth generation of reanalysis climate datasets by the Copernicus Climate Change Service (C3S) at the European Centre for Medium-Range Weather Forecasts (ECMWF) (ECMWF, 2022; Hersbach et al., 2022). Such reanalysis datasets synthesize past-short range weather forecasts and observations to minimize errors (ECMWF, 2022). Reanalysis climate data are widely investigated and used in climate studies from regional to global scales (Hersbach et al., 2020; Hu and Mallorquí, 2019; Naseef and Kumar, 2020; Renfrew et al., 2021; Rodríguez and Bech, 2021; Urraca et al., 2018). ERA5 provides monthly data from 1950 to the present on various climate parameters, such as air temperature and dew-point temperature (Hersbach et al., 2022, 2020). In this study, we used the year 2020 monthly data from the 'ERA5 monthly averaged data on single levels from 1979 to present', which was downloaded as NetCDF format. The spatial resolution of the data is approximately 30 km (0.25 ° latitude and 0.25 ° longitude). We used the monthly dry-bulb temperature (T_{db} [K]) and the dew-point temperature (T_{dew} [K]) in 2020, where these values were directly available from the ERA5 database. These values are measured at 2 m above the surface land, sea, or inland waters (Hersbach et al., 2020). Out of these data, the relative humidity was calculated as follows (Alduchov and Eskridge, 1996):

$$\varphi = 0.01e^{\left(\frac{17.625(T_{dew}-273.15)}{T_{dew}-30.11}-\frac{17.625(T_{db}-273.15)}{T_{db}-30.11}\right)} \tag{28}$$

The downloaded ERA5 data were processed in R (version 4.1.0) (R Core Team, 2020). The entire workflow is depicted in Figure 2. The region of interest (ROI) was cropped. The region outside the ROI was masked out (from a to b in Figure 2). Shapefiles consist of state-level boundaries for India and country-level boundaries for the world. These data were obtained from open-source datasets (Eurostat, 2020; Hijmans, 2022).

3.2 Wet-bulb temperature and temperature depression calculation

The wet-bulb temperature and the maximal temperature depression due to evaporative cooling (c to d in Figure 2) at every single location were calculated as specified in section 1. Since we had the dry-bulb temperature and relative humidity at approximately 30 km resolution, the wet-bulb temperature is also available at this spatial resolution.

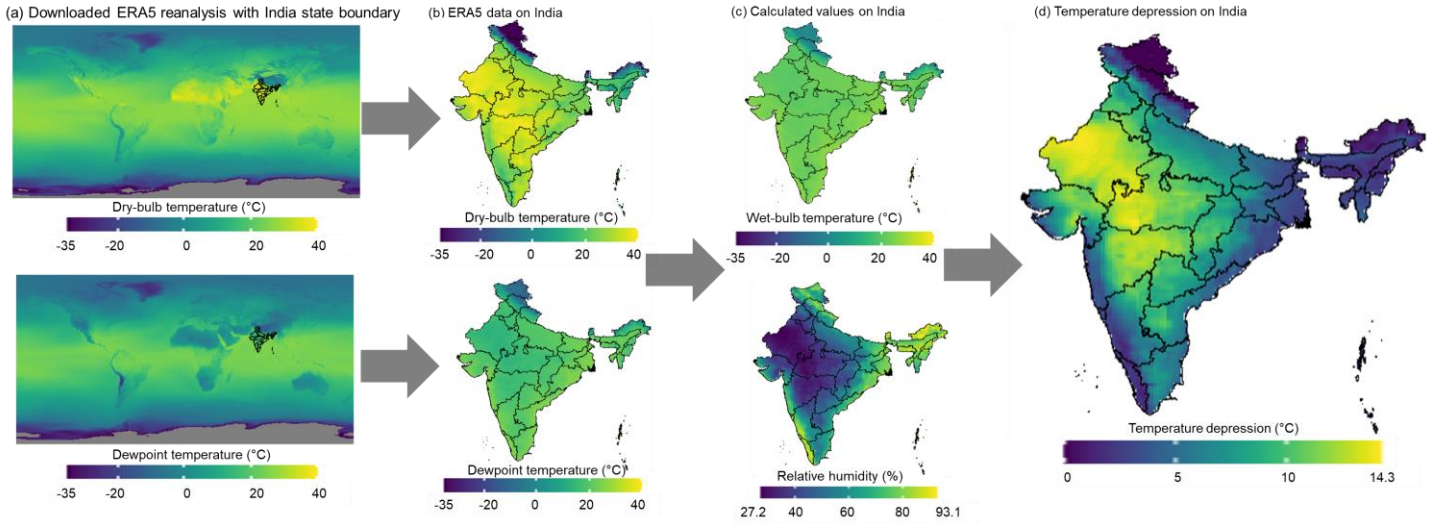

Figure 2. Workflow to obtain the maximal temperature depression by evaporative cooling. The data for May 2020 are used with India as an example: (a) downloaded ERA reanalysis data of dry-bulb and dew-point temperature in °C, together with India state boundaries; (b) ERA5 temperature data, filtered only for India; (c) relative humidity (%), calculated from the temperature, and wet-bulb temperature (°C) for India; (d) derived maximal temperature depression (°C) in India. Note that dry-bulb and dew-point temperatures below -35 °C are shown in grey in (a).

3.3 The gain in postharvest life

The maximal gain in postharvest life that can be obtained by evaporative cooling is calculated. This is done by calculating the postharvest life for storage under ambient (dry-bulb temperature) conditions and calculating the postharvest life when the fresh foods are stored at wet-bulb temperature, so in an idealized evaporative cooler. Both postharvest life calculations are done as detailed for each data point, namely each 30 x 30 km region in India. The workflow to determine this postharvest life gain is shown in Figure 3.

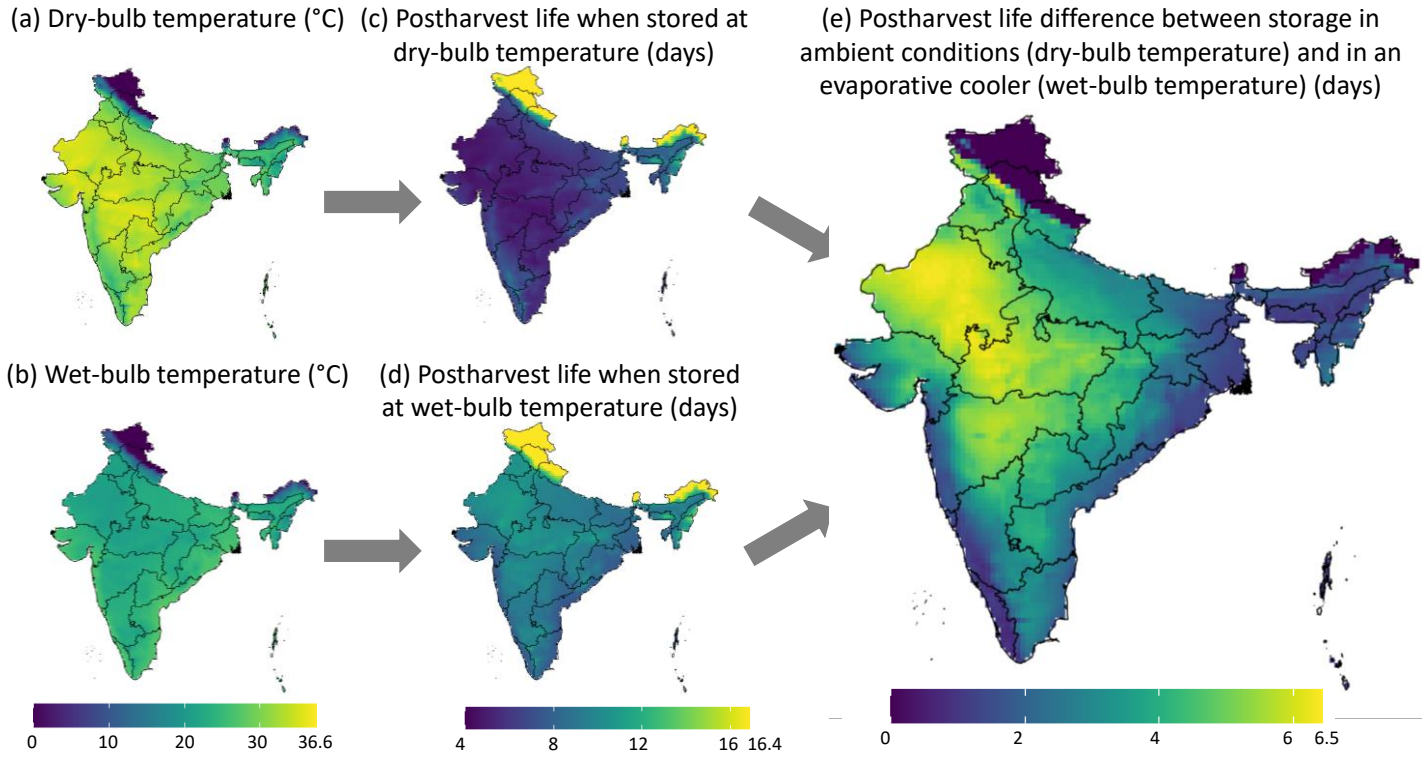

Figure 3. Workflow to obtain the maximal gain in postharvest life evaporative cooling for banana fruit. The data for May 2020 are used in India as an example: (a) dry-bulb temperature, relative humidity and

resulting wet-bulb temperature; (b) postharvest life at ambient conditions and in an evaporative cooler; (c) postharvest life gain throughout India.

3.4 Open access map

We made the data on the temperature depression available online in an open-access map ((Empa, 2022), https://empasimbiosys.github.io/evapo_cooling_map/). The maps are created in R markdown and converted to HTML. These HTML files are in the repository (https://github.com/EmpaSimBioSys/evapo_cooling_map). Some maps have interactive features, such as allowing users to zoom in on the area of interest in the world. The visitors of this map can also compare the difference between the seasons. Such open access map widens the accessibility to the knowledge of evaporative cooling, and it can be updated to include more datasets and features. We plan to advance the maps to meet the needs of users.

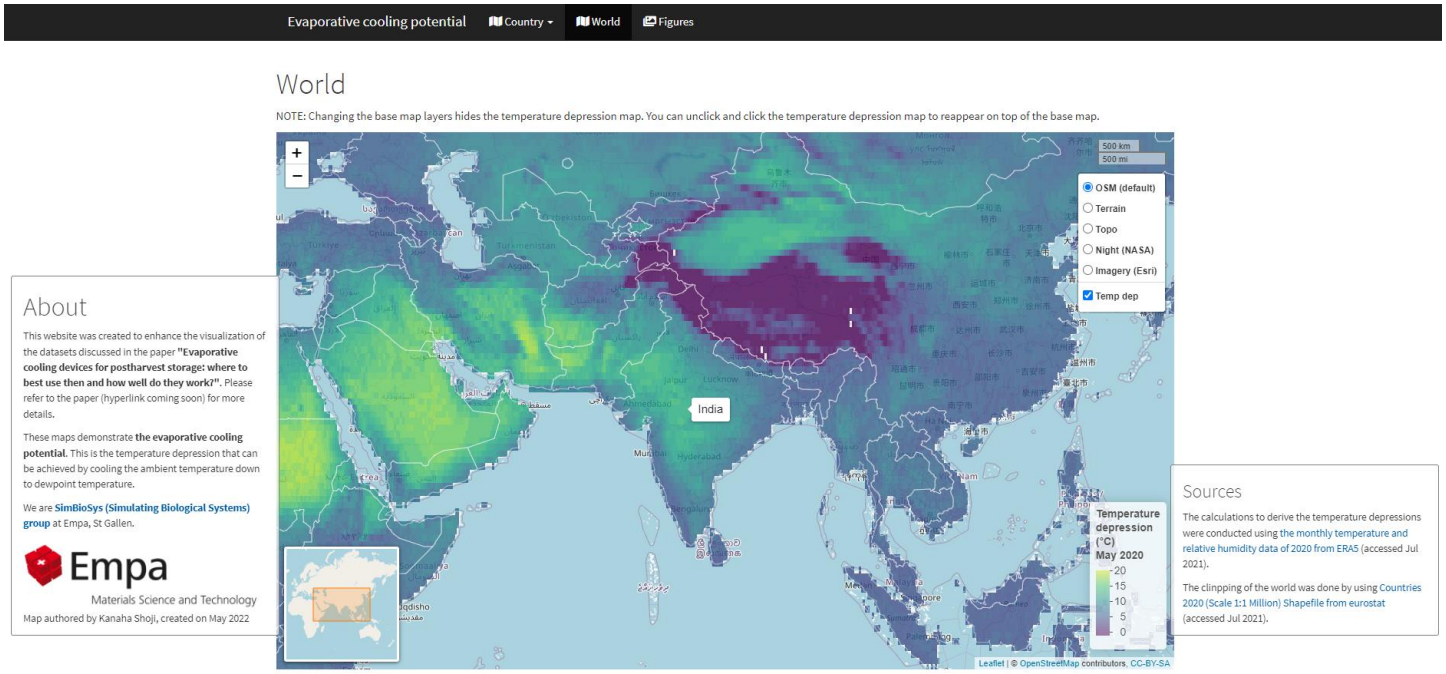

Figure 4. Screenshot of the open-access map.

4 Theory evaporative cooling

4.1 Psychrometrics of evaporative cooling

Evaporative cooling implies that cooling is induced by evaporation, so by the conversion of liquid water to water vapor. Energy is required for the phase change to evaporate water, namely the latent heat of vaporization. This energy is extracted from the air in the form of sensible heat. This heat extraction lowers the temperature of the air. Idealized evaporative cooling is thereby just an energy conversion of sensible heat into latent heat in the air: the sensible heat of the air is lowered as the temperature is reduced, and the latent heat stored in the air increases as more water vapor is present in the air. The enthalpy of the air remains constant, so it is an isenthalpic process.

The wet-bulb temperature is reached for an ideal isenthalpic evaporative cooling process (point B in Figure 4). A maximal conversion of sensible heat into latent heat is reached, thus maximizing the temperature depression. This ideal process implies steady-state conditions, so no heat storage terms, and purely convective heat transfer, so no long-wave radiation or other heat sources. In reality, the process is never fully isenthalpic due to existing other heat sources. As such, the wet-bulb temperature is not exactly reached. The wet-bulb temperature can be determined from psychometric charts or corresponding analytical calculations (Stull, 2011). An iterative calculation to determine the wet-bulb temperature is given in section 1.

The psychrometrics of such an isenthalpic evaporative cooling process can be visualized on a psychrometric chart (Figure 5). First, we identify the initial hygrothermal conditions, namely the dry-bulb temperature and humidity of the environment. These are the air conditions entering the cooler ($T_{db,in}$, φ_{in}). Then we move along the constant-enthalpy line to the final humidity that the air will reach. These isenthalpic lines are parallel to the wet-bulb temperature lines. If the air reaches 100% humidity, the wet-bulb temperature is reached (point B in Figure 5). In reality, the humidity of the air does not reach 100%, which lowers the efficiency of the evaporative cooling process (point C in Figure 5).

The efficiency of the evaporative cooling process (ε_{ec}) is defined as the extent to which the dry-bulb temperature of the air leaving the cooler ($T_{db,out}$ [K]) or cooling pad matches the wet-bulb temperature of the approach flow ($T_{wb,in}$ [K]) (ASHRAE, 2015, 2012; Doğramacı and Aydın, 2020):

$$\varepsilon_{ec} = \frac{T_{db,in} - T_{db,out}}{T_{db,in} - T_{wb,in}} \tag{29}$$

Here $T_{db,in}$ is the dry-bulb temperature of the approach flow [K]. Typical efficiencies for evaporative coolers are between 50-95%.

The sections below define and analyze simplified heat and mass balances for evaporative coolers to quantify the relevant parameters that influence the cooling process and the cooling efficiency. More detailed numerical models for evaporative cooling have been set up (Appropedia, 2021; Rehman et al., 2020).

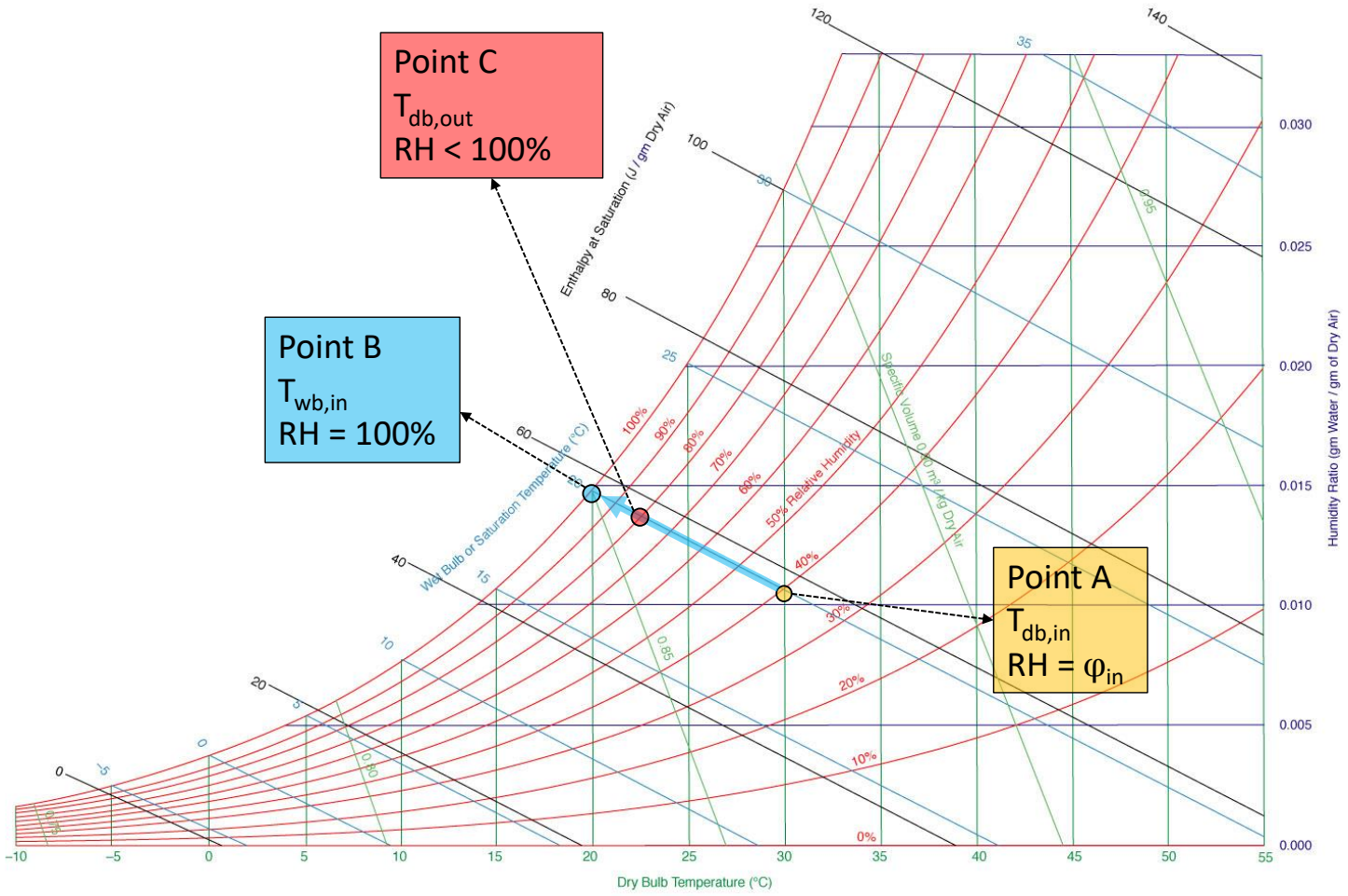

Figure 5. Psychrometric chart with an indication of the evaporative cooling process (adapted from (Ogawa, 2021)***). We depict cooling down to the wet-bulb temperature and 100% relative humidity (Point B) and imperfect cooling to a lower humidity (point C) and a higher temperature.***

4.2 Types of evaporative coolers

Two types of evaporative coolers are described below: (1) a flow-over or evaporative contact cooler, where evaporation occurs at the surface of the cooler; (2) a flow-through evaporative cooler, where evaporation occurs within the cooling pad, as air flows through it.

4.2.1.1 Flow-over or evaporative contact cooling – evaporation from a surface

Evaporative cooling can be achieved by placing the evaporative cooling medium on top of the product that needs to be cooled, such as a fruit box, or wrapping it around the product (Figure 6a). The air flowing over the evaporative cooler cools the cooler's material, which, mainly by conduction, cools the product underneath. When the evaporative cooling process is perfect, the approach flow air gets fully saturated (RH_{out} = φ_{out} = 100%) and reaches the wet-bulb temperature. This occurs, for example, in a channel if the evaporative medium is sufficiently long. Under less ideal conditions, the relative humidity at the outlet will be lower, and the temperature will be higher. Suppose we assume a contact evaporative cooler in steady-state equilibrium conditions. Here we can assume that the temperature of the product to be cooled equals that of the air exiting the evaporative cooler due to the contact cooling. Ideally, this temperature is the wet-bulb temperature then.

Also, non-equilibrium conditions occur in practice, for example, when a new box with warm fruit is placed below the evaporative cooler material. In that case, the evaporative cooling material will cool down due to evaporation and conductively remove heat from the fruit to be cooled. The conductive heat transfer at the product-material interface

is dependent on the temperature gradient at the surface, the conductivity of both materials, and the contact area between the cooler and the product. Note that, in reality, some air can flow inside the evaporative material convectively. In addition, natural convective heat exchange also contributes to cooling to some extent. The reason is that both the evaporative cooling material and the box of fruit have a high macroporosity.

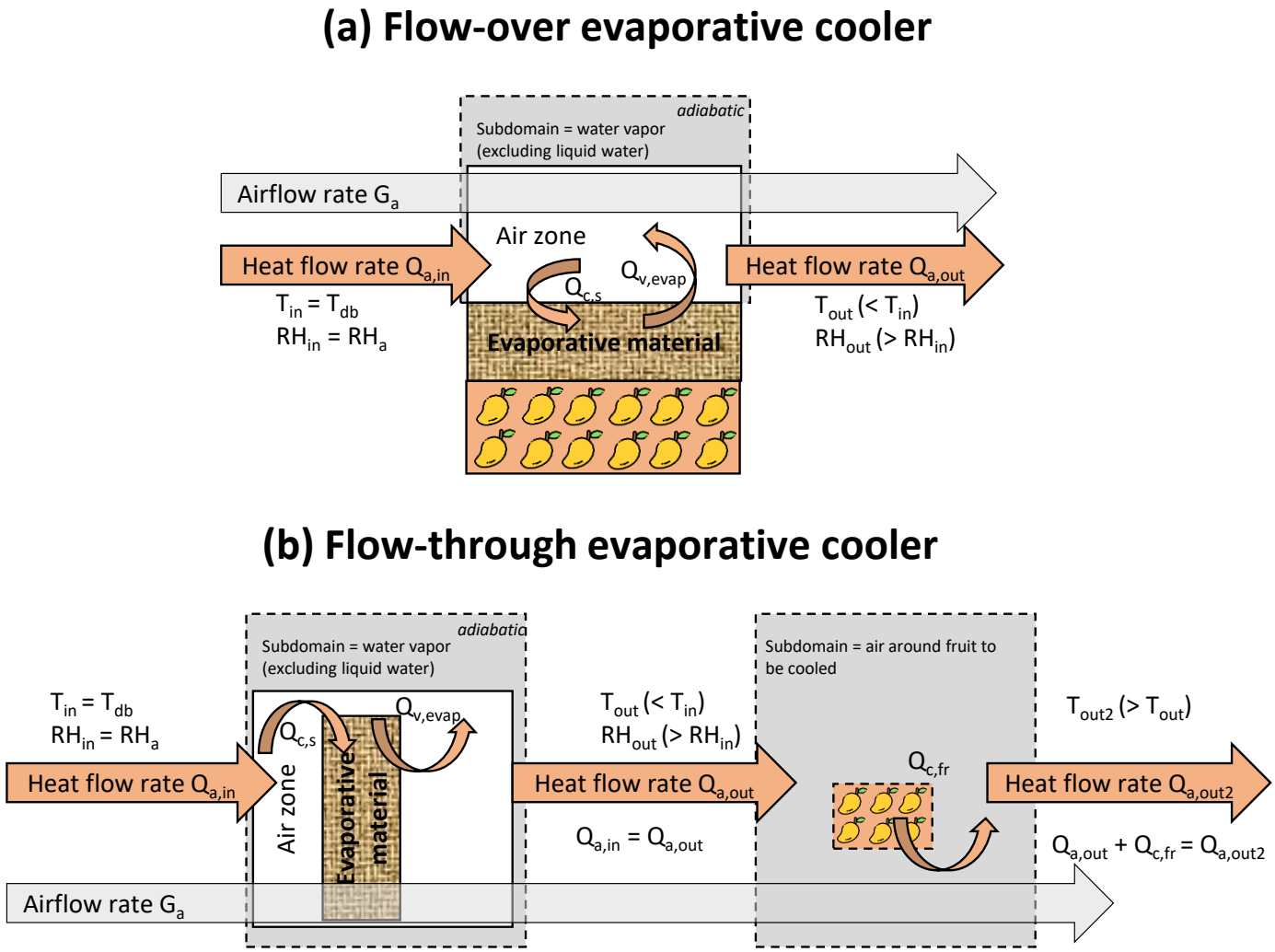

Figure 6. Schematic drawing of a flow-over or evaporative contact cooler and a flow-through cooler.

4.2.1.2 Flow-through evaporative cooling – evaporation through a transfer medium

Evaporative cooling can also be achieved in another way. We can place the evaporative cooling medium or the cooling pad upstream of the material that needs to be cooled, such as a box of fruit (Figure 6b). The air flowing through the evaporative cooler cools the air. This principle is often used with cooling pads. This cold air is then transferred over the product. This air cools the product by convection, not conduction. When the evaporative cooling process is perfect, the approach flow air gets fully saturated (φ_{out} = 100%) and reaches the wet-bulb temperature. This occurs, for example, when the cooling pad is sufficiently thick and the airflow rate is not too high. Under less ideal conditions, the relative humidity exiting the cooler will be lower, and the temperature will be higher than the lower limit, namely the wet-bulb temperature. In steady-state equilibrium conditions, the temperature of the product to be cooled equals that of the air exiting the evaporative cooler. Ideally, this temperature is the wet-bulb temperature then.

Also, non-equilibrium conditions occur in practice, for example, when a new box with warm fruit is placed downstream of the flow-through cooler. In that case, the evaporative cooling material will cool down the air due to evaporation, and this cold air will subsequently convectively remove heat from the fruit to be cooled. The convective heat transfer at the product-material interface ($\dot{Q}_c$) is dependent on the temperature difference between the cold air and the product surface, the convective heat transfer coefficient (CHTC), and the contact area between the cold air and the product, so the surface area of the product $A_{s,fr}$.

$$Q_c = CHTC\left(T_s - T_{out}\right) A_{s,fr} \tag{30}$$

4.3 Mass balance for water vapor in an evaporative cooler

We write the mass balance for water vapor for the convective exchange during evaporative cooling. The system for which we compose the balance is the moist air in a zone around the evaporative cooling material (Figure 7). Liquid water is not included. Instead, evaporation of liquid water into vapor is considered a source term in the vapor balance. This balance holds for both flow-through cooling pads and flow-over contact coolers for the specific system (subdomain):

$$\begin{aligned} G_{v,in} - G_{v,out} + G_{v,evap} &= 0 \\ x_{v,in} G_a - x_{v,out} G_a + G_{v,evap} &= 0 \end{aligned} \tag{31}$$

Here, the mass flow rate of moist air (G_a [kg_a s^{-1}]), volumetric mass flow rate ($\dot{V}_a$ [m_a^3 s^{-1}]) and water vapor flow rate (G_v [kg_v s^{-1}]) are related as follows:

$$G_v = x_v G_a = x_v \rho_a \dot{V}_a \tag{32}$$

Note that the mass and density of moist air can be approximated equal to that of dry air, so $m_a \approx m_d$ and $\rho_a \approx \rho_d$, by which $G_a \approx G_d$. This assumption simplifies further equations since the moist air density ρ_a can now be approximated by ρ_d. This density is independent of the moisture concentration and can be taken as constant or just a function of temperature.

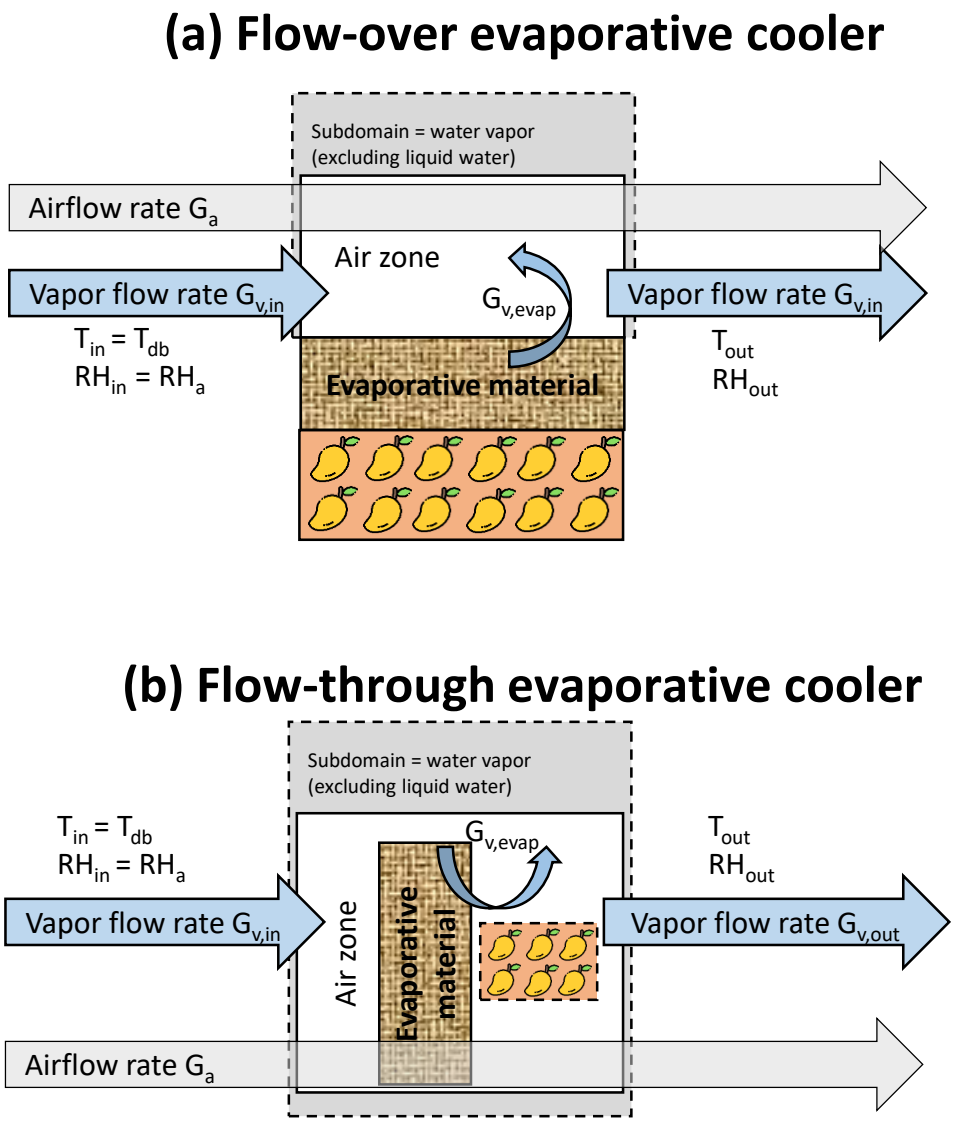

Figure 7. Water vapor mass balance for two types of evaporative coolers: (a) contact cooler; (b) flow-through cooler.

This vapor balance can be rewritten to the evaporation mass flow $G_{v,evap}$:

$$G_{v,evap} = \left(x_{v,out} - x_{v,in} \right) G_a \tag{33}$$

This amount of water that evaporates can be quantified in two ways: (1) by measuring the difference in water vapor fraction between in and outlet; (2) by estimating it from the convective mass exchange at the surface of the evaporative cooling material. The latter can be done in a simplified way by assuming that no internal resistance to liquid or vapor transport is present inside the material, so assuming the material is in the constant drying rate period:

$$G_{v,evap} = CMTC \left(p_{v,s} - p_{v,in} \right) A_s \tag{34}$$

The CMTC is the average convective mass transfer coefficient at the air-material interface within the cooling pad or material [s m^{-1}], A_s is the surface area for mass exchange [m^2], $p_{v,s}$ is the vapor pressure at the surface [Pa], and $p_{v,in}$ is the vapor pressure at the inlet of the evaporative cooler [Pa].

The mass balance can now be rewritten by interchanging the expression for the evaporative mass exchange at the surface.

$$\left(x_{v,out} - x_{v,in}\right) G_a \left\langle U \right\rangle = CMTC \left\langle U \right\rangle \left(p_{v,s} - p_{v,in}\right) A_s \left\langle \phi_{0,bulk}, D_{cc}, D_{ec} \right\rangle \tag{35}$$

Here the angle brackets indicate here the main dependencies to other parameters, such as airspeed (U [m s^{-1}]), the bulk porosity of the charcoal pieces ($\phi_{0,bulk}$), and size of the charcoal pieces (D_{cc}), and the thickness of the cooler wall (D_{ec}).

For idealized evaporative cooling, the temperature at the surface equals the wet-bulb temperature, and the surface of the material is wet so at 100% relative humidity [Pa]. This implies that:

$$p_{v,s} = p_{v,sat}\left(T_s\right) = p_{v,sat}\left(T_{wb}\left\langle T_{db}, \varphi_a \right\rangle\right) \tag{36}$$

As the vapor pressure at the surface equals the saturated vapor pressure $p_{v,sat}$ at the material surface temperature T_s [K]. We can rewrite the equation then as:

$$\left(x_{v,out} - x_{v,in}\right) G_a \left\langle U \right\rangle = CMTC \left\langle U \right\rangle \left(p_{v,sat}\left(T_{wb}\left\langle T_{db}, \varphi_a \right\rangle\right) - p_{v,in}\right) A_s \left\langle \phi_{0,bulk}, D_{cc}, D_{ec} \right\rangle \tag{37}$$

4.4 **Heat balance for an evaporative cooler**

We write the simplified heat balance for the convective exchange of sensible into latent heat during evaporative cooling (Figure 8). The system for which we compose the balance is a zone including the air and the evaporative cooling material. In this system, we assume steady-state conditions and no external heat exchange of the system with the environment (e.g., due to conduction). This system is adiabatic. Since only two heat flows enter the system, the enthalpy of the inlet versus outlet air remains constant. The energy balance for this isenthalpic system can be written as:

$$\begin{aligned} Q_{a,in} - Q_{a,out} &= 0 \\ h_{a,in} G_a - h_{a,out} G_a &= 0 \end{aligned} \tag{38}$$

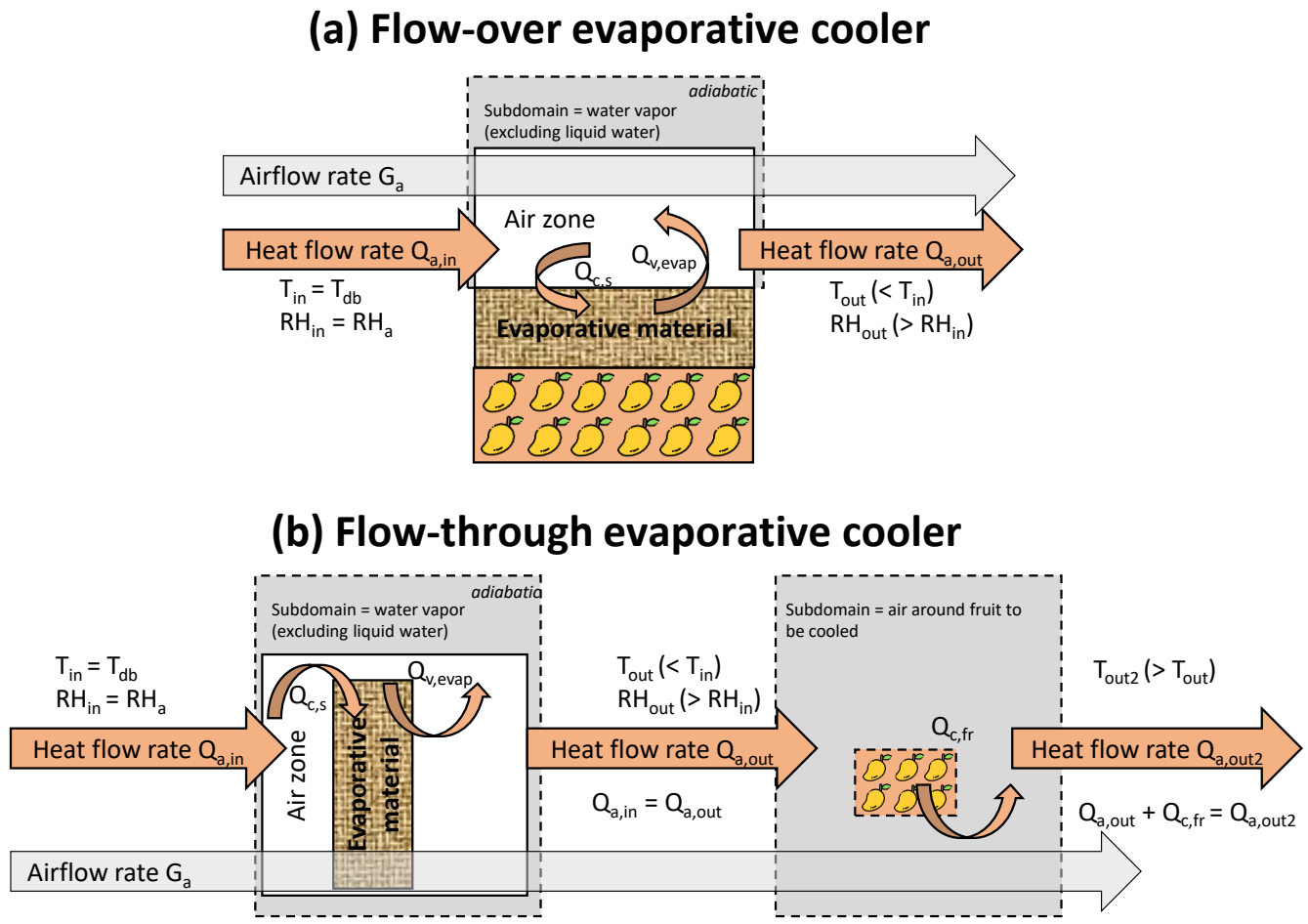

Figure 8. Heat balance for two types of evaporative coolers: (a) contact cooler; (b) flow-through cooler.

This equation assumes that the airflow flow rate at inlet and outlet of the evaporative cooler is the same (G_a[kg_a s^{-1}]). The enthalpy of moist air h_a [J kg_a^{-1}], a gaseous mixture of dry air and water vapor, is defined as:

$$\begin{aligned} h_a &= x_d h_d + x_v h_v \\ h_v &= c_{p,v}\left(T - T_{ref,0}\right) + L_v^{ref} \\ h_d &= c_{p,d}\left(T - T_{ref,0}\right) \end{aligned} \tag{39}$$

where L_v^{ref} is the heat of vaporization or latent heat at $T_{ref,0}$ (2.5 MJ kg^{-1} at $T_{ref,0}$ = 273.15 K, (Engineering-ToolBox, 2010)), $c_{p,v}$ is the specific heat capacity (at constant pressure) of water vapor (1880 J $kg^{-1}K^{-1}$), $c_{p,d}$ specific heat capacity (at constant pressure) of dry air (1006.43 J $kg^{-1}K^{-1}$), x_v is the mass fraction of water vapor in the gaseous phase [kg_v kg_a^{-1}], x_d is the mass fraction of dry air in the gaseous phase [kg_d kg_a^{-1}], h_v is the enthalpy of water vapor [J kg_v^{-1}], h_d is the enthalpy of dry air [J kg_d^{-1}]. Then the heat balance is written as:

$$\begin{aligned} &h_{a,in}G_a - h_{a,out}G_a = 0 \\ &\left(x_{d,in}h_{d,in} + x_{v,in}h_{v,in}\right)G_a = \left(x_{d,out}h_{d,out} + x_{v,out}h_{v,out}\right)G_a \\ &\left[x_{d,in}c_{p,d}\left(T_{db,in} - T_{ref,0}\right) + x_{v,in}\left(c_{p,v}\left(T_{db,in} - T_{ref,0}\right) + L_v^{ref}\right)\right]G_a \\ &= \left[x_{d,out}c_{p,d}\left(T_{db,out} - T_{ref,0}\right) + x_{v,out}\left(c_{p,v}\left(T_{db,out} - T_{ref,0}\right) + L_v^{ref}\right)\right]G_a \end{aligned} \tag{40}$$

The unknowns in this equation are the mass fraction $x_{v,out,}$ and temperature at the outlet $T_{db,out}$. The mass fractions are related by the following relation $x_d = 1\text{-}x_v$. We can simplify this equation, assuming the sensible enthalpy of water

vapor is much smaller than that of dry air. This is realistic since the mass fraction of water vapor is typically much smaller ($x_d >>> x_v \approx 0.005\text{-}0.03$, Figure 5, so $x_d \approx x_a = 1$). In that case, we get:

$$\begin{aligned}
&\left[x_{d,in} c_{p,d} \left(T_{db,in} - T_{ref,0} \right) + x_{v,in} c_{p,v} \left(T_{db,in} - T_{ref,0} \right) + x_{v,in} L_v^{ref} \right] G_a \\
&= \left[x_{d,out} c_{p,d} \left(T_{db,out} - T_{ref,0} \right) + x_{v,out} c_{p,v} \left(T_{db,out} - T_{ref,0} \right) + x_{v,out} L_v^{ref} \right] G_a \\
&\left[x_{d,in} c_{p,d} \left(T_{db,in} - T_{ref,0} \right) + \cancel{x_{v,in} c_{p,v} \left(T_{db,in} - T_{ref,0} \right)} + x_{v,in} L_v^{ref} \right] G_a \\
&= \left[x_{d,out} c_{p,d} \left(T_{db,out} - T_{ref,0} \right) + \cancel{x_{v,out} c_{p,v} \left(T_{db,out} - T_{ref,0} \right)} + x_{v,out} L_v^{ref} \right] G_a
\end{aligned} \tag{41}$$

$$\begin{aligned}
&c_{p,d} \left(T_{db,in} - T_{ref,0} \right) G_a + x_{v,in} L_v^{ref} G_a = c_{p,d} \left(T_{db,out} - T_{ref,0} \right) G_a + x_{v,out} L_v^{ref} G_a \\
&c_{p,d} \left(T_{db,in} - T_{db,out} \right) G_a + \left(x_{v,in} - x_{v,out} \right) L_v^{ref} G_a = 0
\end{aligned} \tag{42}$$

This equation can be rewritten in terms of the evaporated water at the cooler surface $G_{v,evap}$. Thereby, the sensible enthalpy difference between inlet and outlet is directly related to the evaporation process at the surface:

$$c_{p,d} \left(T_{db,in} - T_{db,out} \right) G_a = -\left(x_{v,in} - x_{v,out} \right) L_v^{ref} G_a \tag{43}$$

$$\text{with } -\left(x_{v,in} - x_{v,out} \right) L_v^{ref} G_a = L_v^{ref} \left(x_{v,out} - x_{v,in} \right) G_a = L_v^{ref} G_{evap} = L_v^{ref} CMTC \left(p_{v,s} - p_{v,in} \right) A_s \tag{44}$$

$$c_{p,d} \left(T_{db,in} - T_{db,out} \right) G_a = CMTC \left(p_{v,s} - p_{v,in} \right) A_s L_v^{ref} \tag{45}$$

This equation directly relates the airflow rate G_a to the evaporation process at the surface, so the convective mass transfer rate (CMTC) and the surface area for evaporation of the material that holds the water (A_s). If we also assume that the air becomes fully saturated, so the wet-bulb temperature is reached ($T_{db,out} = T_{wb,in}$), we get from Eq.(42)-(45) :

$$\begin{aligned}
&c_{p,d} \left(T_{db,in} - T_{wb,in} \right) G_a + \left(x_{v,in} - x_{v,out} \left\langle T_{wb,in}, \varphi_a = 100\% \right\rangle \right) L_v^{ref} G_a = 0 \\
&c_{p,d} \left(T_{db,in} - T_{wb,in} \right) G_a = -\left(x_{v,in} - x_{v,out} \left\langle T_{wb,in}, \varphi_a = 100\% \right\rangle \right) L_v^{ref} G_a
\end{aligned} \tag{46}$$

$$c_{p,d} \left(T_{db,in} - T_{wb,in} \right) G_a = CMTC \left(p_{v,sat} \left\langle T_{wb,in} \right\rangle - p_{v,in} \right) A_s L_v^{ref} \tag{47}$$

4.5 Impact on airflow rate on the optimal thickness of the cooler

4.5.1 Background and goals

The airflow rate through an evaporative cooler plays a vital role in its efficiency. It determines the amount of water that is evaporated from the cooler and the resulting temperature depression. The airflow rate thereby also determines the increase in air humidity. In addition to the efficiency of the evaporative cooler ε_{ec} [-] the airflow rate also determines its evaporative cooling capacity Q_{evap} [W]. The efficiency and cooling capacity are calculated by:

$$\varepsilon_{ec} = \frac{T_{db,in} - T_{db,out}}{T_{db,in} - T_{wb,in}} \tag{48}$$

$$Q_{evap} = -L_v^{ref} G_{evap} \tag{49}$$

Here, the subscripts in and out represent the conditions of the air that flows in and out of the evaporative cooler unit, respectively. If the airflow rate through the cooler is high, the volume of warm air becomes too large to be fully cooled down. The air does not become saturated, and the temperature does not reach the wet-bulb temperature, so the efficiency drops. We cool down a larger air volume to a higher temperature than theoretically possible with evaporative cooling. In addition, a high airflow rate will deplete the water in the charcoal faster than required, consuming more water. The evaporative cooling material will go faster from the constant drying rate period (CDRP) to the decreasing

drying rate period (DDRP). During the DDRP, the water evaporation is thereby limited by the transport in the material, slowing down the process. This internal resistance to water transport reduces the water flow from the material and will strongly limit the efficiency of the evaporative cooler. Charcoal, for example, has a pore structure that leads to a long CDRP, which is beneficial. The efficiency will be lower at high airflow rates, but the cooling capacity (Q_{evap}) will be high as the water evaporation rate is high. Experiments confirmed that at high airflow rates, we get a higher outlet temperature exiting an evaporative cooler, a lower humidity, and a high cooling capacity (Doğramacı and Aydın, 2020). The lower relative humidity will lead to more wilting of the fruit or vegetables in the evaporative cooler.

If the airflow rate is low, the air will become saturated, and the air temperature will reach the wet-bulb temperature. In that case, the evaporative cooling efficiency (ε_{ec}) will be optimal. In reality, however, the wet-bulb temperature is often not reached at low airflow rates since convection is not the main heat transfer mechanism that plays a role. Other heat transfer processes also contribute, such as long-wave radiation. At low airflow rates, much less water is evaporated, by which the evaporative cooling capacity (Q_{evap}) is often not maximized. As such, there is an optimal airflow rate through the evaporative cooler.

A trade-off exists for the airflow rate between maximizing the cooling efficiency (Eq.(48)) versus maximizing cooling capacity (Eq.(49)). These criteria require rather low airflow rates versus high airflow rates passing through the cooler. An optimal mass flow rate can be determined for evaporative coolers, similar to what was done by (Doğramacı and Aydın, 2020) for the cooling of buildings. For evaporative coolers for fruit storage, the priorities in choosing the flow rate are different than for buildings. During the precooling process, a high cooling capacity can bring the product temperature down to remove the field heat. Here a high cooling capacity could be prioritized over a high cooling efficiency. However, evaporative cooling is more relevant for longer-term cold storage of fruit cooling over several days. In that case, reaching the lowest possible temperature is essential to reduce the decay reactions in the fruit. Therefore, maximizing the evaporative cooling efficiency is often preferred over a high cooling capacity once the fruit is cooled down.

4.5.2 Optimal cooler design for local airflow conditions

In reality, we cannot control the airflow rate in passive evaporative coolers as the local wind speeds determine it. The occurrence of these airspeeds throughout the year can be evaluated using the wind rose at a specific location, the height above the ground, and the atmospheric boundary layer in that region, which is illustrated in Figure 9. (Defraeye and Carmeliet, 2010). We should thereby design the thickness of an evaporative cooler to reach the optimal cooling efficiency under the local airflow conditions at that specific location. The accessible surface area of the material for evaporation, such as charcoal pieces, is relevant here when we assume air can flow through the porous structure. This implies a sufficient open porous stacking of the charcoal pieces and a permeable textile membrane, for example, a charcoal cooler (Defraeye et al., 2022). If the size or surface area for mass exchange is too low, air will not be saturated. Then the air temperature will not reach the wet-bulb temperature.

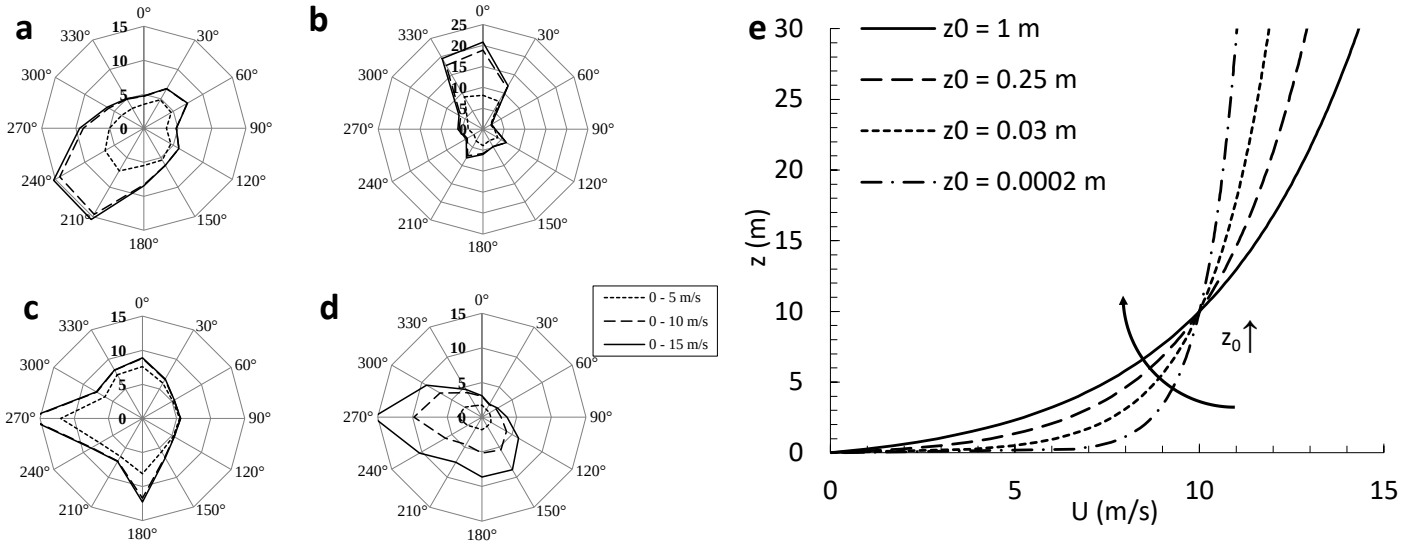

Figure 9. Wind conditions measured at the meteorological stations in: (a) Eindhoven (The Netherlands); (b) Ferrel (Portugal); (c) Granada (Spain); (d) Cairngorm (United Kingdom). Percentage of occurrence (indicated in bold) of wind speeds for different wind speed intervals at specific wind directions (north 0º, east 90º). The data are obtained from the European Wind Atlas (Troen and Petersen, 1989)***. Note that the scale of Ferrel differs from that of Granada and Cairngorm. (e) Atmospheric boundary layer, namely mean horizontal wind speed (U) as a function of height (z) for different terrain roughness' (z_0) height. Figures adjusted from*** (Defraeye and Carmeliet, 2010)**.**

The optimal airflow rate for maximizing the cooling efficiency (G_a [kg s^{-1}]) was determined in section 4.5.3, out of the heat balance of the evaporative cooler:

$$G_a\left\langle U\right\rangle = CMTC\left\langle U\right\rangle \frac{\left(p_{v,sat}\left\langle T_{wb,in}\left\langle T_{db,in},\varphi_a\right\rangle\right\rangle - p_{v,in}\left\langle T_{db,in},\varphi_a\right\rangle\right)}{c_{p,d}\left(T_{db,in}-T_{wb,in}\left\langle T_{db,in},\varphi_a\right\rangle\right)} A_s L_v^{ref} \tag{50}$$

Here, the CMTC is the convective mass transfer coefficient at the air-material interface [s m^{-1}], U is the approach flow airspeed impinging the cooler [m s^{-1}], and A_s is the surface area of the evaporative material for mass exchange inside the evaporative cooler, for example, the surface area of charcoal pieces [m^2]. This equation is only valid under steady-state conditions with no external heat exchange of the system with the environment, so an adiabatic system. The equation also assumes that the air becomes fully saturated after moving through the evaporative cooler. This case implies idealized evaporative cooling. We rewrote and simplified this equation as a function of the surface area of the evaporative material for mass exchange and the airspeed required to reach this optimal point (section 4.5.3). We simplified the equation also using the psychrometric constant. As such, the equation becomes independent of T_{db} and φ_a. Finally, we get:

$$A_s\left\langle \phi_{0,bulk}, D_{cc}, D_{ec}\right\rangle = \frac{A_{ec}\cdot U\cdot \rho_a\cdot \varepsilon}{CMTC\left\langle U\right\rangle \cdot P_{atm}} \tag{51}$$

This surface area needs to be determined iteratively since the CMTC within the porous medium is also a function of the airspeed. This ideal surface area can now be calculated as a function of $\phi_{0,bulk,}$ and D_{ec}, for charcoal pieces of a size $D_{cc.}$ The equations to calculate the CMTC and the specific surface area A_s are given in section 4.7. Out of these equations, the optimal thickness of an evaporative cooler can be determined (section 4.5.3):

$$D_{ec} = \frac{U\cdot \rho_a\cdot \varepsilon}{CMTC\left\langle U\right\rangle \cdot P_{atm}\cdot A_{sf}\left\langle \phi_{0,bulk}, D_{cc}\right\rangle} \tag{52}$$

Here, A_{sf} is the surface area of the evaporative material for mass exchange per volume unit of the cooler [m^2 m^{-3}].

4.5.3 Optimal cooler design for local airflow conditions: Detailed calculation

Out of the heat balance of the evaporative cooler, the optimal airflow rate for maximizing the cooling efficiency can be determined. This mass flow rate to reach this equilibrium equals:

$$G_a\left\langle U\right\rangle = CMTC\left\langle U\right\rangle \frac{\left(p_{v,sat}\left\langle T_{wb,in}\left\langle T_{db,in},\varphi_a\right\rangle\right\rangle - p_{v,in}\left\langle T_{db,in},\varphi_a\right\rangle\right)}{c_{p,d}\left(T_{db,in}-T_{wb,in}\left\langle T_{db,in},\varphi_a\right\rangle\right)} A_s L_v^{ref} \tag{53}$$

Here, the dependency of the mass flow rate and the CMTC to the airspeed U is indicated and other main dependencies. This equation assumes that no internal resistance to liquid or vapor transport in the evaporative material exists. We are in the constant drying rate period where the vapor pressure at the material surface equals the saturated vapor pressure. A maximal enthalpy conversion of latent heat into sensible heat occurs at this airflow rate. The wet-bulb temperature conditions are reached, and the air is quasi-saturated with water vapor. The outlet temperature increases at a higher flow rate, and the efficiency decreases. The wet-bulb temperature can also be reached at a lower airflow rate than specified in Eq.(53). The cooling capacity will be lower in this case.

We rewrite and simplify this equation as a function of the surface area for mass exchange and the airspeed that is required to reach this optimal point. To do so, we scaled the airflow rate per square meter of an evaporative cooler, so the mass flux of moist air g_a [kg m^{-2} s^{-1}]:

$$g_a\left\langle U\right\rangle = \frac{G_a\left\langle U\right\rangle}{A_{ec}} = \frac{A_s}{A_{ec}} CMTC\left\langle U\right\rangle \frac{\left(p_{v,sat}\left\langle T_{wb,in}\left\langle T_{db,in},\varphi_a\right\rangle\right\rangle - p_{v,in}\left\langle T_{db,in},\varphi_a\right\rangle\right)}{c_{p,d}\left(T_{db,in}-T_{wb,in}\left\langle T_{db,in},\varphi_a\right\rangle\right)} L_v^{ref} \tag{54}$$

With the air density, we can calculate the average airspeed through the cooler:

$$U = \frac{g_a}{\rho_a} = \frac{1}{\rho_a}\frac{A_s\left\langle \phi_{0,bulk}, D_{cc}, D_{ec}\right\rangle}{A_{ec}} CMTC\left\langle U\right\rangle \frac{\left(p_{v,sat}\left\langle T_{wb,in}\left\langle T_{db,in},\varphi_a\right\rangle\right\rangle - p_{v,in}\left\langle T_{db,in},\varphi_a\right\rangle\right)}{c_{p,d}\left(T_{db,in}-T_{wb,in}\left\langle T_{db,in},\varphi_a\right\rangle\right)} L_v^{ref} \tag{55}$$

This equation can be rewritten using the psychrometric constant γ (≈ 0.65 x 10^{-3} K^{-1}):

$$\gamma = \frac{c_{p,d}}{L_v^{ref}\frac{M_v}{M_d}} = \frac{c_{p,d}}{L_v^{ref}\varepsilon} = \frac{1}{P_{atm}} \frac{\left(p_{v,sat}\left\langle T_{wb,in}\left\langle T_{db,in},\varphi_a\right\rangle\right\rangle - p_{v,in}\left\langle T_{db,in},\varphi_a\right\rangle\right)}{\left(T_{db,in}-T_{wb,in}\left\langle T_{db,in},\varphi_a\right\rangle\right)} \tag{56}$$

We rewrite the equation then accordingly:

$$U = \frac{g_a}{\rho_a} = \frac{1}{\rho_a}\frac{A_s\left\langle \phi_{0,bulk}, D_{cc}, D_{ec}\right\rangle}{A_{ec}} CMTC\left\langle U\right\rangle \gamma P_{atm} \frac{L_v^{ref}}{c_{p,d}} \tag{57}$$

The equation can be simplified to determine the airspeeds that are required to reach this optimal point and wet-bulb temperature conditions for a flow-through evaporative cooler:

$$U = \frac{1}{\rho_a}\frac{A_s\left\langle \phi_{0,macro}, D_{cc}, D_{ec}\right\rangle}{A_{ec}} CMTC\left\langle U\right\rangle \gamma P_{atm} \frac{L_v^{ref}}{c_{p,d}} \tag{58}$$

$$\begin{aligned} U &= \frac{1}{\rho_a}\frac{A_s\left\langle \phi_{0,macro}, D_{cc}, D_{ec}\right\rangle}{A_{ec}} CMTC\left\langle U\right\rangle \gamma P_{atm} \frac{L_v^{ref}}{c_{p,d}} \\ &= \frac{1}{\rho_a}\frac{A_s\left\langle \phi_{0,macro}, D_{cc}, D_{ec}\right\rangle}{A_{ec}} CMTC\left\langle U\right\rangle \left(\frac{c_{p,d}}{L_v^{ref}\varepsilon}\right) P_{atm} \frac{L_v^{ref}}{c_{p,d}} \end{aligned} \tag{59}$$

$$U = \frac{1}{\rho_a}\frac{A_s\left\langle \phi_{0,macro}, D_{cc}, D_{ec}\right\rangle}{A_{ec}} CMTC\left\langle U\right\rangle \frac{P_{atm}}{\varepsilon} = \frac{1}{\rho_a}\frac{A_s\left\langle \phi_{0,macro}, D_{cc}, D_{ec}\right\rangle}{A_{ec}} CMTC\left\langle U\right\rangle \frac{P_{atm}}{\frac{M_v}{M_d}} \tag{60}$$

$$= \frac{1}{\rho_a}\frac{A_s\left\langle \phi_{0,macro}, D_{cc}, D_{ec}\right\rangle}{A_{ec}} CMTC\left\langle U\right\rangle \frac{P_{atm}}{0.622}$$

This airspeed is thereby independent of T_{db} and φ_a . This airspeed needs to be determined iteratively since the CMTC within the porous medium is also a function of the airspeed. This ideal airspeed can be displayed as a function of $\phi_{0,bulk}$ and D_{cc}. The equations to calculate the CMTC and the specific surface area A_s are given in section 4.7. We can also determine the surface area of charcoal in an evaporative cooler that is required to achieve these equilibrium conditions for a given airspeed:

$$A_s\left\langle \phi_{0,bulk}, D_{cc}, D_{ec}\right\rangle = \frac{A_{ec}\cdot U\cdot \rho_a \cdot \varepsilon}{CMTC\left\langle U\right\rangle \cdot P_{atm}} \tag{61}$$

Out of these equations, the optimal thickness of an evaporative cooler can be determined D_{ec}:

$$A_s\left\langle \phi_{0,bulk}, D_{cc}, D_{ec}\right\rangle = A_{sf}\left\langle \phi_{0,bulk}, D_{cc}\right\rangle D_{ec}A_{ec} = \frac{A_{ec}\cdot U\cdot \rho_a \cdot \varepsilon}{CMTC\left\langle U\right\rangle \cdot P_{atm}}$$

$$A_{sf}\left\langle \phi_{0,bulk}, D_{cc}\right\rangle D_{ec}A_{ec} = \frac{A_{ec}\cdot U\cdot \rho_a \cdot \varepsilon}{CMTC\left\langle U\right\rangle \cdot P_{atm}} \tag{62}$$

$$D_{ec} = \frac{U\cdot \rho_a \cdot \varepsilon}{CMTC\left\langle U\right\rangle \cdot P_{atm}\cdot A_{sf}\left\langle \phi_{0,bulk}, D_{cc}\right\rangle}$$

Here, A_{sf} is the surface area of the evaporative material for mass exchange per volume unit of the cooler [$m^2\,m^{-3}$].

4.6 **Heat balance at the air-material interface for isenthalpic evaporation**

Within the evaporative cooler system, the isenthalpic conversion of sensible heat into latent heat comes from the internal energy balance at the surface of the evaporative cooler. Note that, in reality also other heat sources need to be accounted for, such as long-wave radiation or conduction. This balance (Figure 8) actually states that the convective heat extracted from the air at the surface ($Q_{c,s}$ [J s^{-1}]) equals the latent heat supplied by the evaporation of water ($Q_{v,evap}$ [J s^{-1}]). This energy balance is detailed as:

$$\begin{aligned} &Q_{c,s} - Q_{v,evap} = 0 \\ &CHTC\left(T_s - T_{db,in}\right)A_s - \left(-L_v^{ref}G_{evap}\right) = 0 \\ &CHTC\left(T_s - T_{db,in}\right)A_s + CMTC\left(p_{v,s} - p_{v,in}\right)A_s L_v^{ref} = 0 \end{aligned} \tag{63}$$

For an evaporative cooler placed in a channel or as a flow-through cooling pad, this equation is rewritten. If we assume steady-state conditions and that the air becomes fully saturated, so the wet-bulb temperature is reached ($T_s = T_{wb}$), we get:

$$CHTC\left(T_{wb,in} - T_{db,in}\right)A_{s,h} + CMTC\left(p_{v,sat}\left\langle T_{wb,in}\right\rangle - p_{v,in}\right)A_{s,v}L_v^{ref} = 0 \tag{64}$$

$$CHTC\left(T_{wb,in}\left\langle T_{db,in}, \varphi_a\right\rangle - T_{db,in}\right)A_{s,h} + CMTC\left(p_{v,sat}\left\langle T_{wb,in}\left\langle T_{db,in}, \varphi_a\right\rangle\right\rangle - p_{v,in}\left\langle T_{db,in}, \varphi_a\right\rangle\right)A_{s,v}L_v^{ref} = 0 \tag{65}$$

Here $A_{s,h,}$ and $A_{s,v}$ are the surface areas for heat and mass exchange, respectively. This heat exchange at the surface determines how much the temperature will drop and how much the temperature will rise. Apart from the hygrothermal inlet conditions, the key influence parameters are the convective transfer coefficients and the surface

area for heat and mass exchange. Here the CHTC and CMTC are directly dependent on the airspeed so the airflow rate. If the surface area for heat and mass exchange is the same, the equation becomes:

$$CHTC\left(T_{wb,in}\left\langle T_{db,in},\varphi_a\right\rangle - T_{db,in}\right) + CMTC\left(p_{v,sat}\left\langle T_{wb,in}\left\langle T_{db,in},\varphi_a\right\rangle\right\rangle - p_{v,in}\left\langle T_{db,in},\varphi_a\right\rangle\right)L_v^{ref} = 0 \tag{66}$$

This equation can be rewritten as the ratio of the transfer coefficients:

$$\frac{CMTC}{CHTC} = -\frac{\left(T_{wb,in}\left\langle T_{db,in},\varphi_a\right\rangle - T_{db,in}\right)}{\left(p_{v,sat}\left\langle T_{wb,in}\left\langle T_{db,in},\varphi_a\right\rangle\right\rangle - p_{v,in}\left\langle T_{db,in},\varphi_a\right\rangle\right)L_v^{ref}} = \frac{\left(T_{db,in} - T_{wb,in}\left\langle T_{db,in},\varphi_a\right\rangle\right)}{\left(p_{v,sat}\left\langle T_{wb,in}\left\langle T_{db,in},\varphi_a\right\rangle\right\rangle - p_{v,in}\left\langle T_{db,in},\varphi_a\right\rangle\right)L_v^{ref}} \tag{67}$$

Note that the ratio of the transfer coefficients is almost constant for different environmental conditions (T. Defraeye et al., 2012). This equation can be rewritten using the psychrometric constant as well.

$$\frac{CMTC}{CHTC} = \frac{\left(T_{db,in} - T_{wb,in}\left\langle T_{db,in},\varphi_a\right\rangle\right)}{\left(p_{v,sat}\left\langle T_{wb,in}\left\langle T_{db,in},\varphi_a\right\rangle\right\rangle - p_{v,in}\left\langle T_{db,in},\varphi_a\right\rangle\right)L_v^{ref}} = \frac{1}{\gamma P_{atm} L_v^{ref}} \tag{68}$$

$$\frac{CMTC}{CHTC} = \frac{1}{\gamma P_{atm} L_v^{ref}} = \frac{\varepsilon}{c_{p,d} P_{atm}} \tag{69}$$

4.7 Convective mass transfer coefficient and surface area for evaporation

We estimate the CMTC and the specific surface area A_{sf} in a simplified way. If we assume uniform spherical particles, the specific surface area A_{sf} [$m^2\ m^{-3}$] is calculated as:

$$A_{sf} = \frac{A_{cc,uc}}{V_{t,uc}} = \frac{A_{cc,uc}}{V_{cc,uc}}\left(1-\phi_{0,bulk}\right) = \frac{4\pi R_{cc}^{\ 2}}{\frac{4}{3}\pi R_{cc}^{\ 3}}\left(1-\phi_{0,bulk}\right) = \frac{3}{R_{cc}}\left(1-\phi_{0,bulk}\right) \tag{70}$$

Here $A_{cc,uc}$ is the surface area of the charcoal in a unit cell containing a spherical particle, $V_{cc,uc}$ is the volume of that particle in the unit cell, and V_t is the total volume of the unit cell. When we use the example of our previously-designed evaporative cooler (Defraeye et al., 2022), the specific surface area is estimated from the porosity (61%), the diameter of the charcoal pieces (80 mm). These values lead to A_{sf} = 29 $m^2\ m^{-3}$. The corresponding surface area of charcoal in one square meter of evaporative cooler (A_{ec} = 1 m^2) with a thickness of 100 mm equals 2.9 m^2 ($A_s = A_{sf} \,.\, A_{ec} \,.\, D_{ec}$). In reality, the effective porosity could be lower than predicted, as we assume perfectly spherical particles, whereas charcoal pieces are often irregular in shape and size.

The convective mass transfer coefficient (CMTC) is calculated from a correlation of the convective heat transfer coefficient (CHTC) with the airspeed and the analogy between heat and mass transfer. The average CHTC for a packed bed of porous pieces is calculated as a function of the Reynolds and the Prandtl number (section 4.8):

$$\mathrm{CHTC} = \frac{\lambda_a}{d_p}\frac{1-\phi_{0,\mathrm{bulk}}}{\phi_{0,\mathrm{bulk}}}\left(0.5\left(\frac{\mathrm{U}d_p}{\nu_a\left(1-\phi_{0,\mathrm{bulk}}\right)}\right)^{0.5} + 0.2\left(\frac{\mathrm{U}d_p}{\nu_a\left(1-\phi_{0,\mathrm{bulk}}\right)}\right)^{0.667}\right)\mathrm{Pr}^{0.33} \tag{71}$$

4.8 Convective heat transfer coefficient for a packed bed

Convective heat transfer coefficients quantify the convective heat exchange between the charcoal and the airflow. This coefficient is mainly dependent on the charcoal piece size, shape, and airspeed approaching the charcoal. We evaluate existing correlations for airflow in a packed bed of spherical pieces. We obtain an average CHTC over the entire charcoal surface. The following correlation is available for flow in a packed bed of spherical particles (Whitaker, 1972):

$$\mathrm{Nu_{pb}} = \left(0.5\,\mathrm{Re_{pb}}^{0.5} + 0.2\,\mathrm{Re_{pb}}^{0.667}\right)\mathrm{Pr}^{0.33} \tag{72}$$

The parameters in this equation are:

$$\begin{aligned}
Nu_{pb} &= \frac{CHTC.L_{ref,pb}}{\lambda_a} = \frac{CHTC.d_p}{\lambda_a}\frac{\phi_{0,bulk}}{1-\phi_{0,bulk}} \\
\mathrm{Re}_{pb} &= \frac{V_{pb}.L_{ref,pb}}{\nu_a} = \frac{\frac{U_{pb}}{\phi_{0,bulk}}.d_p\frac{\phi_{0,bulk}}{1-\phi_{0,bulk}}}{\nu_a} = \frac{U_{pb}.d_p}{\nu_a\left(1-\phi_{0,bulk}\right)} \\
L_{ref,pb} &= d_p\frac{\phi_{0,bulk}}{1-\phi_{0,bulk}} \\
V_{pb} &= \frac{U_{pb}}{\phi_{0,bulk}} \\
d_p &= \frac{6V_p}{A_p} = \frac{6\frac{4}{3}\pi r_p^{\,3}}{4\pi r_p^{\,2}} = \frac{6r_p}{3} = 2r_p \\
CHTC &= \frac{Q_{c,s}}{A_{s,h}}\left(T_s - T_{db,in}\right)
\end{aligned} \tag{73}$$

Pr is the Prandtl number, ν_a is the kinematic viscosity of air [$m^2\ s^{-1}$], V_{pb} is the physical airspeed in the packed bed [$m\ s^{-1}$], U_{pb} is the superficial airspeed in the packed bed [$m\ s^{-1}$], $L_{ref,pb}$ is the characteristic length of the packed bed [m], λ_a is the thermal conductivity of the air [$W\ m^{-1}\ K^{-1}$], r_p is the radius of the particles [m]. Re_{pb} is the particle Reynolds number in the packed bed, in which the characteristic length scale is a measure of the size of the void spaces (Whitaker, 1972). Nu_{pb} is the particle Nusselt number in a packed bed. Both Reynolds and Nusselt numbers are a function of the porosity, which implies that the impact of the void space and packing density on the airflow and corresponding heat transfer is included in the correlations. $T_{db,in}$ is the approach flow temperature of the air that enters the packed bed. T_s is the surface temperature of the material. Note that these empirical correlations were derived for forced convection, so buoyancy effects were not explicitly accounted for. These are dependent on the temperature difference between the air and the fruit. The packed bed correlation was derived for a Re_{pb} range from 22 – 8 000. This correlation can be rewritten directly as a function of the CHTC:

$$CHTC = \frac{\lambda_a}{d_p}\frac{1-\phi_{0,bulk}}{\phi_{0,bulk}}Nu_{pb} \tag{74}$$

$$\begin{aligned}
\mathrm{CHTC} &= \frac{\lambda_a}{d_p}\frac{1-\phi_{0,bulk}}{\phi_{0,bulk}}\left(0.5\,\mathrm{Re_{pb}}^{0.5} + 0.2\,\mathrm{Re_{pb}}^{0.667}\right)\mathrm{Pr}^{0.33} \\
&= \frac{\lambda_a}{d_p}\frac{1-\phi_{0,bulk}}{\phi_{0,bulk}}\left(0.5\left(\frac{\frac{U_{pb}}{\phi_{0,bulk}}.d_p\frac{\phi_{0,bulk}}{1-\phi_{0,bulk}}}{\nu_a}\right)^{0.5} + 0.2\left(\frac{\frac{U_{pb}}{\phi_{0,bulk}}.d_p\frac{\phi_{0,bulk}}{1-\phi_{0,bulk}}}{\nu_a}\right)^{0.667}\right)\mathrm{Pr}^{0.33}
\end{aligned} \tag{75}$$

This equation enables us to calculate the CHTC directly from the superficial airspeed, porosity, particle diameter, and air properties:

$$\mathrm{CHTC} = \frac{\lambda_a}{d_p}\frac{1-\phi_{0,bulk}}{\phi_{0,bulk}}\left(0.5\left(\frac{U_{pb}d_p}{\nu_a\left(1-\phi_{0,bulk}\right)}\right)^{0.5} + 0.2\left(\frac{U_{pb}d_p}{\nu_a\left(1-\phi_{0,bulk}\right)}\right)^{0.667}\right)\mathrm{Pr}^{0.33} \tag{76}$$

4.9 What is the COP of an evaporative cooler?

The coefficient of performance (COP) of an evaporative cooler can be defined as equivalent to that of a refrigerator. It is defined as the total power released by the evaporative cooler (Q_{evap} [J s^{-1}]), which is the evaporated heat extracted from the air, by the total heat that can be used to cool all the fruit in the evaporative cooler $Q_{ec,fr}$ [J s^{-1}]:

$$COP = \frac{Q_{v,evap}}{Q_{c,fr}} = \frac{L_v^{ref} G_{v,evap}}{CHTC_{fr}\left(T_{s,fr} - T_{out}\right) A_{fr}} \tag{77}$$

Here $T_{s,fr}$ is the surface temperature of the fruit, and T_{out} is the temperature that exists the evaporative cooler surface and impinges onto the fruit. This COP will vary over time as the fruits start to cool down and the fruit temperature converges to the temperature of the impinging air (T_{out}). Less energy from the cold air will then be transferred to the fruit.

Nomenclature

Symbols

A_s	surface area of the evaporative material for mass exchange [m^2]
$A_{cc,uc}$	surface area of the charcoal in a unit cell containing a spherical particle [m^2]
A_{ec}	frontal area of evaporative cooler, perpendicular to flow direction [m^2]
A_{sf}	surface area of the evaporative material for mass exchange, per volume unit of the cooler [$m^2\ m^{-3}$]
c_p	specific heat capacity (at constant pressure) [$J\ kg^{-1}K^{-1}$]
CHTC	convective transfer coefficient [$W\ m^{-2}\ K^{-1}$]
CMTC	convective mass transfer coefficient at the air-material interface [$s\ m^{-1}$]
d_p	diameter of particle [m]
D_{cc}	average caliber (size) of the charcoal so equivalent diameter or sieve size [m]
D_{ec}	thickness of an evaporative cooling pad [m]
E_a	activation energy [$J\ mol^{-1}$]
E_{ec}	energy extracted by evaporative cooler [J]
E_{lat}	energy needed by latent heat for evaporation [J]
g	gravitational acceleration [$m\ s^{-2}$]
g_a	mass flux of moist air [$kg_a\ m^{-2}\ s^{-1}$]
G_a	mass flow rate of moist air [$kg_a\ s^{-1}$]
G_v	mass flow rate of water vapor [$kg_v\ s^{-1}$]
$G_{v,evap}$	evaporated water at the cooler material surface [$kg_v\ s^{-1}$]
h_a	enthalpy of moist air [$J\ kg_a^{-1}$]
h_d	enthalpy of dry air [$J\ kg_d^{-1}$]
h_v	enthalpy of water vapor [$J\ kg_v^{-1}$]
I	overall fruit quality index [-]
k_{fr}	temperature-dependent rate constant of the fruit [s^{-1}]
k_0	pre-exponential reference rate constant [s^{-1}]
L	length scale [m]
L_v^{ref}	latent heat of vaporization at T_{ref} [$J\ kg_l^{-1}$]
m_a	mass of moist air [kg]
m_d	mass of dry air [kg]
m_{fr}	mass of the fruit [kg]
m_l	mass of liquid water [kg]
m_v	mass of water vapor [kg]
M_a	molecular mass of moist air [$g\ mol^{-1}$]
M_d	molecular mass of dry air [$g\ mol^{-1}$]
M_v	molecular mass of water vapor [$g\ mol^{-1}$]
Nu	Nusselt number [-]

p_a	total pressure of moist air [Pa]
p_d	partial pressure of dry air [Pa]
p_v	partial pressure of water vapor [Pa]
$p_{v,sat}$	saturated vapor pressure [Pa]
PL	postharvest life of fresh produce [d]
ΔPL	maximal gain in postharvest life of fresh produce [d]
P_{atm}	atmospheric pressure [Pa]
P_{ec}	evaporative cooling power [J s^{-1}]
Pr	Prandtl number [-]
Q_a	heat in the air [J s^{-1}]
$Q_{c,s}$	convective heat extracted from the air at the product interface [J s^{-1}]
$Q_{ec,fr}$	heat that can be used to cool all the fruit in the evaporative cooler [J s^{-1}]
Q_{evap}	heat extracted from evaporation of water so evaporative cooling capacity [J s^{-1}]
Q_{10}	Q_{10} value [-]
R	universal gas constant [J mol^{-1} K^{-1}]
R_a	specific gas constants of moist air [J $kg^{-1}K^{-1}$]
R_d	specific gas constants of dry air [J $kg^{-1}K^{-1}$]
R_v	specific gas constants of water vapor [J $kg^{-1}K^{-1}$]
Re	Reynolds number [-]
r_p	radius of the particles [m]
t	time [s]
T	temperature in Kelvin [K]
ΔT_{ev}	maximal temperature depression achieved by evaporative cooling [K]
U	air speed [m s^{-1}]
U_{ref}	approach flow air speed [m s^{-1}]
U_{pb}	superficial air speed in the packed bed [m s^{-1}]
V	volume [m^3]
V_{pb}	physical air speed in the packed bed [m s^{-1}]
$V_{cc,uc}$	volume of a particle in a unit cell [m^3]
V_t	total volume of the unit cell [m^3]
$\dot{V}_a$	volumetric flow rate of moist air [m_a^3 s^{-1}]
w_s	solid material matrix content of porous material [kg m_{PM}^{-3}]
w_{PM}	moisture (liquid and vapor) content of porous material [kg m_{PM}^{-3}]
X	dry-base moisture (liquid and vapor) content of porous material [kg kg_{dm}^{-1}]
x_d	mass fraction of dry air [kg_d kg_a^{-1}]
x_v	mass fraction of water vapor or specific humidity [kg_v kg_a^{-1}]

x_v'	mass fraction of water vapor or specific humidity defined per unit of dry air [$kg_v\ kg_d^{-1}$]
$\langle\ \rangle$	dependent variables are placed within angle brackets

Greek symbols

Δ	difference, interval
ε	ratio of molecular weight of water and dry air [$kg_v\ kg_d^{-1}$]
ε_{ec}	efficiency of the evaporative cooler [-]
γ	psychrometric constant [K^{-1}]
λ	thermal conductivity [$W\ m^{-1}\ K^{-1}$]
φ	relative humidity [-]
θ	Temperature in degrees Celsius [ºC]
ρ_a	density of moist air [$kg_a\ m_a^{-3}$]
ρ_d	density of dry air [$kg_d\ m_a^{-3}$]
ρ_v	density of water vapor or absolute humidity [$kg_v\ m_a^{-3}$]
$\phi_{0,bulk}$	bulk porosity of the porous material [-]
ν	kinematic viscosity [$m^2\ s^{-1}$]

Subscripts

a	moist air
atm	atmosphere
bulk	bulk
cc	charcoal
d	dry air
dew	dew-point
db	dry-bulb
evap	evaporated
eq	equilibrium
ec	evaporative cooler
fr	fruit
guess_0	initial value for the iterative calculation
h	heat
ini	initial
in	inflow
l	liquid
lat	latent
out	outflow
pb	packed bed

ref	reference conditions
s	surface
sat	saturated
t	total
thr	threshold for quality loss
uc	unit cell
v	vapor
wb	wet-bulb

Abbreviations

AF	analogy factor
CHTC	convective transfer coefficient
CMTC	convective mass transfer coefficient at the air-material interface
COP	coefficient of performance
PL	postharvest life
ΔPL	difference in postharvest life due to evaporative cooling
RH	relative humidity

REFERENCES

Alduchov, O.A., Eskridge, R.E., 1996. Improved Magnus form approximation of saturation vapor pressure. J. Appl. Meteorol. Climatol. 35, 601–609. https://doi.org/https://doi.org/10.1175/1520-0450(1996)035<0601:IMFAOS>2.0.CO;2

Allen, R., Pereira, L., Raes, D., Smith, M., 1998. Crop evapotranspiration - Guidelines for computing crop water requirements - FAO Irrigation and drainage paper 56, Evapotranspiración del cultivo Guías para la determinación de los requerimientos de agua de los cultivos. ESTUDIO FAO RIEGO Y DRENAJE 56. Rome.

Appropedia, 2021. Charcoal Cooler [WWW Document]. URL https://www.appropedia.org/Charcoal_Cooler

ASHRAE, 2015. ANSI/ASHRAE Standard 133-2015: Method of Testing Direct Evaporative Air Coolers.

ASHRAE, 2012. ASHRAE Handbook - HVAC Systems and Equipment.

Camelo, A.F.L., 2004. Manual for the preparation and sale of fruits and vegetables [WWW Document]. FAO.

Cantwell, M., 2001. Properties and recommended conditions for long-term storage of fresh fruits and vegetables.

Defraeye, T., Blocken, B., Carmeliet, J., 2012. Analysis of convective heat and mass transfer coefficients for convective drying of a porous flat plate by conjugate modelling. Int. J. Heat Mass Transf. 55, 112–124. https://doi.org/10.1016/j.ijheatmasstransfer.2011.08.047

Defraeye, Thijs, Blocken, B., Carmeliet, J., 2012. Analysis of convective heat and mass transfer coefficients for convective drying of a porous flat plate by conjugate modelling. Int. J. Heat Mass Transf. 55, 112–124. https://doi.org/10.1016/j.ijheatmasstransfer.2011.08.047

Defraeye, T., Carmeliet, J., 2010. A methodology to assess the influence of local wind conditions and building orientation on the convective heat transfer at building surfaces. Environ. Model. Softw. 25. https://doi.org/10.1016/j.envsoft.2010.06.002

Defraeye, T., Radu, A., 2017. Convective drying of fruit: A deeper look at the air-material interface by conjugate modeling. Int. J. Heat Mass Transf. 108, 1610–1622. https://doi.org/10.1016/j.ijheatmasstransfer.2017.01.002

Defraeye, T., Schudel, S., Shrivastava, C., Motmans, T., Umani, K., Crenna, E., Shoji, K., Onwude, D., 2022. The charcoal cooling blanket: A scalable, simple, self-supporting evaporative cooling device for preserving fresh foods. engrXiv. https://doi.org/https://engrxiv.org/preprint/view/2221

Defraeye, T., Tagliavini, G., Wu, W., Prawiranto, K., Schudel, S., Assefa Kerisima, M., Verboven, P., Bühlmann, A., 2019. Digital twins probe into food cooling and biochemical quality changes for reducing losses in refrigerated supply chains. Resour. Conserv. Recycl. 149, 778–794. https://doi.org/10.1016/j.resconrec.2019.06.002

Doğramacı, P.A., Aydın, D., 2020. Comparative experimental investigation of novel organic materials for direct evaporative cooling applications in hot-dry climate. J. Build. Eng. 30, 101240. https://doi.org/10.1016/j.jobe.2020.101240

ECMWF, 2022. ECMWF Reanalysis v5 | ECMWF_ERA5 [WWW Document]. URL https://www.ecmwf.int/en/forecasts/datasets/reanalysis-datasets/era5

Eissa, A.H.A., Gomaa, A.H., Maksoud, M.A.E.A. El, Saeidy, E.A.E. El, Sisi, S.F. El, 2017. Simplified Heat and Mass Transfer Modeling for Anna Apples Cold Storage. http://www.sciencepublishinggroup.com 1, 17. https://doi.org/10.11648/J.IJFET.20170101.13

Engineering-ToolBox, 2010. Water - Heat of Vaporization [WWW Document]. URL https://www.engineeringtoolbox.com/water-properties-d_1573.html

Eurostat, 2020. Countries - GISCO - Eurostat [WWW Document]. URL https://ec.europa.eu/eurostat/web/gisco/geodata/reference-data/administrative-units-statistical-units/countries

Hersbach, H., Bell, B., Berrisford, P., Biavati, G., Horányi, A., Muñoz Sabater, J., Nicolas, J., Peubey, C., Radu, R., Rozum, I., Schepers, D., Simmons, A., Soci, C., Dee, D., Thépaut, J.-N., 2022. ERA5 hourly data on single levels from 1979 to present. [WWW Document]. Copernicus Clim. Chang. Serv. Clim. Data Store. URL https://cds.climate.copernicus.eu/cdsapp#!/dataset/reanalysis-era5-single-levels?tab=overview

Hersbach, H., Bell, B., Berrisford, P., Hirahara, S., Horányi, A., Muñoz-Sabater, J., Nicolas, J., Peubey, C., Radu, R., Schepers, D., Simmons, A., Soci, C., Abdalla, S., Abellan, X., Balsamo, G., Bechtold, P., Biavati, G., Bidlot, J., Bonavita, M., Chiara, G. De, Dahlgren, P., Dee, D., Diamantakis, M., Dragani, R., Flemming, J., Forbes, R., Fuentes, M., Geer, A., Haimberger, L., Healy, S., Hogan, R.J., Hólm, E., Janisková, M., Keeley, S., Laloyaux, P., Lopez, P., Lupu, C., Radnoti, G., Rosnay, P. de, Rozum, I., Vamborg, F., Villaume, S., Thépaut, J.-N., 2020. The ERA5 global reanalysis. Q. J. R. Meteorol. Soc. 146, 1999–2049. https://doi.org/10.1002/QJ.3803

Hijmans, R.J., 2022. First-level Administrative Divisions, India, 2015 - GeoWeb [WWW Document]. Univ. California, Berkeley. Museum Vertebr. Zool. URL https://maps.princeton.edu/catalog/stanford-mw277wc3858

Hu, Z., Mallorquí, J.J., 2019. An Accurate Method to Correct Atmospheric Phase Delay for InSAR with the ERA5 Global Atmospheric Model. Remote Sens. 2019, Vol. 11, Page 1969 11, 1969. https://doi.org/10.3390/RS11171969

Knox, J.A., Nevius, D.S., Knox, P.N., 2017. Two Simple and Accurate Approximations for Wet-Bulb Temperature in Moist Conditions, with Forecasting Applications. Bull. Am. Meteorol. Soc. 98, 1897–1906. https://doi.org/10.1175/BAMS-D-16-0246.1

Kole, N.K., Prasad, S., 1994. Respiration rate and heat of respiration of some fruits under controlled atmosphere conditions. Int. J. Refrig. 17, 199–204. https://doi.org/10.1016/0140-7007(94)90019-1

Naseef, T.M., Kumar, V.S., 2020. Climatology and trends of the Indian Ocean surface waves based on 39-year long ERA5 reanalysis data. Int. J. Climatol. 40, 979–1006. https://doi.org/10.1002/JOC.6251

Ogawa, A., 2021. Psychrometric chart at sea level in SI units [WWW Document]. URL https://commons.wikimedia.org/wiki/File:PsychrometricChart-SeaLevel-SI.jpg

R Core Team, 2020. R: A Language and Environment for Statistical Computing.

Rehman, D., McGarrigle, E., Glicksman, L., Verploegen, E., 2020. A heat and mass transport model of clay pot evaporative coolers for vegetable storage. Int. J. Heat Mass Transf. 162, 120270. https://doi.org/10.1016/j.ijheatmasstransfer.2020.120270

Renfrew, I.A., Barrell, C., Elvidge, A.D., Brooke, J.K., Duscha, C., King, J.C., Kristiansen, J., Cope, T.L., Moore, G.W.K., Pickart, R.S., Reuder, J., Sandu, I., Sergeev, D., Terpstra, A., Våge, K., Weiss, A., 2021. An evaluation of surface meteorology and fluxes over the Iceland and Greenland Seas in ERA5 reanalysis: The impact of sea ice distribution. Q. J. R. Meteorol. Soc. 147, 691–712. https://doi.org/10.1002/QJ.3941

Robertson, G.L., 2016. Food Packaging: Principles and Practice, Third Edit. ed. Taylor & Francis Group LLC, Boca-Raton. https://doi.org/10.1177/0340035206070163

Rodríguez, O., Bech, J., 2021. Tornadic environments in the Iberian Peninsula and the Balearic Islands based on ERA5 reanalysis. Int. J. Climatol. 41, E1959–E1979. https://doi.org/10.1002/JOC.6825

Shoji, K., Schudel, S., Onwude, D., Shrivastava, C., Defraeye, T., 2022. Mapping the postharvest life of imported fruits from packhouse to retail stores using physics-based digital twins. Resour. Conserv. Recycl. 176, 105914. https://doi.org/10.1016/j.resconrec.2021.105914

Simões-Moreira, J.R., 1999. A thermodynamic formulation of the psychrometer constant. Meas. Sci. Technol 10, 302–311.

Stull, R., 2011. Wet-bulb temperature from relative humidity and air temperature. J. Appl. Meteorol. Climatol. 50, 2267–2269. https://doi.org/10.1175/JAMC-D-11-0143.1

Tijskens, L.M.M., Polderdijk, J.J., 1996. A generic model for keeping quality of vegetable produce during storage and distribution. Agric. Syst. 51, 431–452. https://doi.org/10.1016/0308-521X(95)00058-D

Troen, I., Petersen, E.L., 1989. European Wind Atlas. Roskilde, Denmark.

Urraca, R., Huld, T., Gracia-Amillo, A., Martinez-de-Pison, F.J., Kaspar, F., Sanz-Garcia, A., 2018. Evaluation of global horizontal irradiance estimates from ERA5 and COSMO-REA6 reanalyses using ground and satellite-based data. Sol. Energy 164, 339–354. https://doi.org/10.1016/J.SOLENER.2018.02.059

Whitaker, S., 1972. Forced convection heat transfer correlations for flow in pipes, past flat plates, single cylinders, single spheres, and for flow in packed beds and tube bundles. AIChE J. 18, 361–371. https://doi.org/10.1002/aic.690180219